

**STABILITY ANALYSIS OF JEFFERY-HAMEL SIMILARITY SOLUTION
AND ITS RELATION TO FLOW IN A DIVERGING CHANNEL**

by

Al-Maruf Khan

Roll: 1018092501F, Registration No: 1018092501

Session: October, 2018

MASTER OF SCIENCE
IN
MATHEMATICS



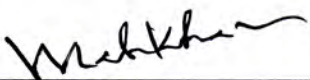
Department of Mathematics
Bangladesh University of Engineering and Technology, Dhaka-1000
March-2021

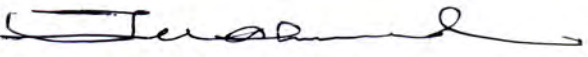
The Thesis Titled
**STABILITY ANALYSIS OF JEFFERY-HAMEL SIMILARITY SOLUTION
AND ITS RELATION TO FLOW IN A DIVERGING CHANNEL**


Submitted by
Al-Maruf Khan

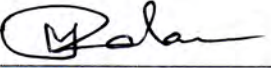
Student No: 1018092501F, Registration No: 1018092501, Session: October 2018, has been accepted as satisfactory in partial fulfillment of the requirement for the degree of Master of Science in Mathematics on 7 March 2021.

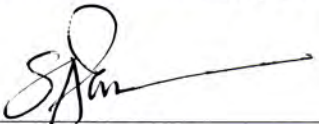
BOARD OF EXAMINERS

1. 

Dr. Md. Abdul Hakim Khan
Professor
Department of Mathematics, BUET, Dhaka-1000
Chairman
(Supervisor)
2. 

Dr. Khandker Farid Uddin Ahmed
Professor and Head
Department of Mathematics, BUET, Dhaka-1000
Member
(Ex-Officio)
3. 

Dr. Md. Abdul Alim
Professor
Department of Mathematics, BUET, Dhaka-1000
Member
4. 

Dr. Md. Mustafizur Rahman
Professor
Department of Mathematics, BUET, Dhaka-1000
Member
5. 

Dr. Md. Sarwar Alam
Professor
Department of Mathematics, Jagannath University, Dhaka-1000
Member
(External)

AUTHOR'S DECLARATION

I hereby announce that the work which is being presented in this thesis entitled '**STABILITY ANALYSIS OF JEFFERY-HAMEL SIMILARITY SOLUTION AND ITS RELATION TO FLOW IN A DIVERGING CHANNEL**' submitted in partial fulfillment of the requirements for the degree of **Master of Science** in Mathematics on March 2021, Bangladesh University of Engineering and Technology, Dhaka-1000 is my work with proper citation and acknowledgement.

It is hereby declared that this thesis or any part of it has not been submitted elsewhere for any degree or diploma.

Al-Maruf Khan

Al-Maruf Khan

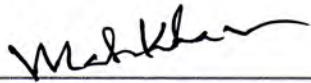
M. Sc. Student

Department of Mathematics

Bangladesh University of Engineering and Technology, Dhaka-1000

CERTIFICATE OF RESEARCH

This is certified that the work entitled '**STABILITY ANALYSIS OF JEFFERY-HAMEL SIMILARITY SOLUTION AND ITS RELATION TO FLOW IN A DIVERGING CHANNEL**' has been carried out by Al-Maruf Khan under the supervision of Dr. Md. Abdul Hakim Khan, Professor, Department of Mathematics, Bangladesh University of Engineering and Technology, Dhaka-1000.

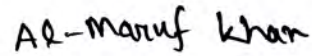


Dr. Md. Abdul Hakim Khan

Professor

Department of Mathematics

BUET, Dhaka-1000



Al-Maruf Khan

Student No: 1018092501F

Session: October 2018

Status: Full-time

Dedicated
to
My Parents

ACKNOWLEDGEMENT

I have the privilege to express my deep respect, gratitude, and sincere appreciation to my supervisor Professor Dr. Md. Abdul Hakim Khan, Department of Mathematics, Bangladesh University of Engineering and Technology, Dhaka who has initiated me into the realm of mathematical research. Without his valuable guidance, constant encouragement, and generous help it was difficult to complete this thesis. I am grateful to him allow me to work with him as a research student and for every effort that he made to get me on the right track of the thesis.

I would like to my heartiest gratitude to Dr. Khandker Farid Uddin Ahmed, Professor, and Head, Department of Mathematics, Bangladesh University of Engineering and Technology, for his expert guidance and valuable suggestions. I would like to express my sincere thanks and gratitude to Professor Dr. Md. Abdul Alim and Professor Dr. Md. Mustafizur Rahman for their encouragement and providing all sorts of co-operations and suggestions. I would like to extend my sincere thanks to all other respected teachers of this department for their valuable comments, inspiration, time to time guidance, and providing all necessary help during M.Sc. degree.

I wish thanks to the staff of the Department of Mathematics, BUET, for their cooperation in this work.

I would like to thank the Ministry of Science and Technology, Government of the People's Republic of Bangladesh for providing NST fellowship during this work.

Finally, I want to express my gratefulness to the Almighty Allah for enabling me to complete the work successfully.

ABSTRACT

Stability analysis of Jeffery-Hamel similarity solution and its relation to flow in a Diverging Channel is studied numerically in this thesis. Numerical results are presented for the two-dimensional flow in a wedge separated by an angle 2α and bounded by circular arcs at the inlet/outlet for radial outflow of the fluid. The Physical problem is presented mathematically governed by a non-dimensional form of equations with appropriate boundary conditions. Hence it is solved by employing the Finite Element Method and Hermite-Padé Approximant Method.

The investigations are reported for different parameters such as Reynolds number, angles, and inlet/outlet radius ratio parameter. These results are presented graphically in the form of streamlines and velocity profiles. Also, the stability of the solutions is shown by pitchfork bifurcation and $\alpha - Re$ relation for two different kinds of inlet profiles. Comparisons with previously published results are performed and the results are found to be in excellent agreement.

TABLE OF CONTENTS

Items	Page
BOARD OF EXAMINERS	ii
CERTIFICATE OF RESEARCH	iv
ACKNOWLEDGEMENT	vi
ABSTRACT	vii
NOMENCLATURE	xi
LIST OF TABLE	xii
LIST OF FIGURES	xii
CHAPTER 1	1
INTRODUCTION	1
1.1 Overview of Viscous Flows in Sectors and Domains with Corners	1
1.1.1 Jeffery –Hamel Flows	3
1.2 Stability Analysis for Systems	6
1.3 Basic Concepts of Bifurcation Analysis	10
1.3.1 The Pitchfork Bifurcation	10
1.3.2 Hopf Bifurcation	12
1.4 Objectives of the Present Work	14
1.5 Organization of the Thesis	15
CHAPTER 2	16
COMPUTATIONAL TECHNIQUE	16

2.1 Numerical Solution Method of Computational FluidDynamics.....	17
2.1.1 Mathematical Model	17
2.1.2 Discretization Method.....	17
2.1.3 Numerical Grid.....	17
2.1.4 Finite Approximations	18
2.1.5 Solution Technique	18
2.2 Discretization Approaches.....	18
2.2.1 Finite Element Method.....	19
2.2.2 Mesh Generation	20
2.2.3 Computational Procedure of Finite Element Formulation	21
CHAPTER 3.....	24
MATHEMATICAL MODELLING.....	24
3.1 General.....	24
3.2 Physical Configurations.....	24
3.3 MathematicalFormulation.....	25
3.3.1 Governing equations	25
3.3.2 Dimensional Analysis	27
3.4 NumericalAnalysis.....	30
3.4.1 Mathematical Formulation for Finite Element Method	30
3.4.1.1 Variation of Inlet Condition	31
3.4.2 Hermite-Pade Approximant Solution	32
3.4.3 Validation of numerical scheme.....	32

CHAPTER 4	34
RESULTS AND DISCUSSION.....	34
4.1 Effect of angle (α).....	34
4.2 Effect of Reynolds number (Re).....	38
4.3 Effect of radius ratio (η).....	42
4.4 The Bifurcation Structure in Finite Domain.....	45
4.5 The Physical Relevance of Numerical results.....	47
CHAPTER 5	49
CONCLUSION.....	49
5.1 Summary of the Major Outcome.....	49
FUTURE WORK.....	50
References.....	51

NOMENCLATURE

\widehat{R}_i	Inlet Radius
\widehat{R}_o	Outlet Radius
Re	Reynolds Number
Q	Constant Radial Volume Flux
\widehat{Re}_c	Critical Values of Reynolds Number
U_{max}	Maximum Centerline Velocity
r	Radial Distance from the Source

Greek Symbols

η	Radius Ratio
α	Elevation Angle
θ	Azimuthal Direction in Cylindrical Co-ordinate
ψ	Stream Function
ν	Kinematic Viscosity

Abbreviations

CFD	Computational Fluid Dynamics
PDE	Partial Differential Equation
FDM	Finite Difference Method
FVM	Finite Volume Method
FEM	Finite Element Method
PTF	Pseudo Traction Free

LIST OF TABLE

Table 4.1: The variation of the critical Reynolds \widehat{Re}_c number of the symmetry-breaking bifurcation in a finite domain.....	47
--	----

LIST OF FIGURES

Figure 1.1: Flow in a sector	2
Figure 1.2: The Flow regimes II_1 , II_2 , IV_1 and V_1	3
Figure 1.3: A Schematic diagram of the $\alpha - Re$ relation (Frankel [8])	4
Figure 1.4: Diagram corresponding to pitchfork bifurcation.....	12
Figure 1.5: Diagram corresponding to Holf bifurcation	14
Figure 2.1: A typical two-dimensional Finite Element mesh (Reddy and Gartling [25])	20
Figure 2.2: Flow chart of computational procedure	21
Figure 3.1: Geometry for Jeffery-Hamel flow	25
Figure 3.2: Code validation of the present research	33
Figure 4.1: Effect of α on velocity profile at $\eta = 100$	36
Figure 4.2: Effect of α on streamlines at $\eta = 100$	37
Figure 4.3: Effect of Re on velocity profiles	40
Figure 4.4: Effect on Re on streamlines	41
Figure 4.5: Effect of η on velocity profiles	43
Figure 4.6: Effect of η on streamlines	44
Figure 4.7: Critical relationship in the $\alpha - Re$ plane for $0 \leq Re \leq 60$	46
Figure 4.8: Critical relationship in $\alpha - Re$ plane for $20 \leq Re \leq 120$	47

CHAPTER 1

INTRODUCTION

Fluid dynamics is a wide branch of science. One of the most basic and well-studied models of fluid dynamics is the incompressible viscous fluid model. It is described by the system of Navier-Stokes equations. The Navier-Stokes equations form the nonlinear system of partial differential equations (PDEs). It is well-known that the Navier-Stokes system cannot be solved analytically in the general case. Its analytical solutions are rarely available in the literature and have been found only for the very basic problem formulations. That is why most of the current research in fluid dynamics is based on the computational approach (or on the experimental one).

This trend can be observed in research on the problem of viscous fluid flow in sectors. The flow between two nonparallel walls is common in practical situations. It may be considered one of the most important problems in fluid mechanics due to a wide range of applications. Viscous, incompressible flow in a two-dimensional wedge, frequently referred to as Jeffery-Hamel flow. The first analytical solutions of this problem in a very simple formulation were found almost a century ago [1, 2]. Since then, several aspects of the problem have been studied and other related problem formulations have been considered in the literature [3, 4, 5, 6]; with most of the works used either purely numerical methods or both analytic and numerical methods.

1.1 Overview of Viscous Flows in Sectors and Domains with Corners

Fluid flows in sectors and domains with corners have a wide range of applications including mechanical engineering, aerospace, and water flow in rivers and canals. Such flows occur whenever there is a plane corner or a conic apex in the flow domain, or when the domain has sector-like or conic outlets to infinity.

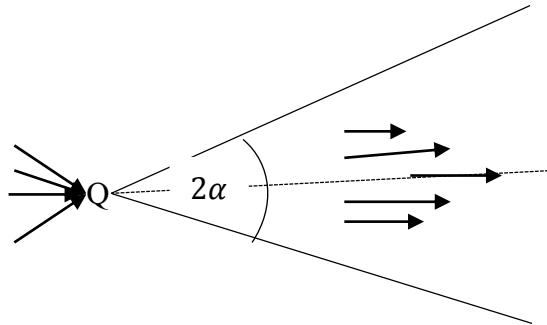


Figure 1.1: Flow in a sector

The mathematical formulation of a problem of flow in sectors has three main dimensionless parameters (see Figure 1.1):

- the sector opening angle 2α ,
- the constant radial volume flux Q ,
- and the Reynolds number Re .

There are two types of flow in sectors:

- 1) flows due to a source ($Q = 1$) or a sink ($Q = -1$) at the corner point
- 2) flows with zero net flow rate ($Q = 0$) due to some disturbance

The first type of flows is related to so-called Jeffery-Hamel flows and will be discussed in Sub-Section 1.1.1

1.1.1 Jeffery –Hamel Flows

Mathematical modelling of flows in sectors has a long history. The first works were done independently by Jeffery [1] and Hamel [2] in the beginning of the previous century. They considered the problem in the simplest formulation and found a class of 2D steady radial flows due to a source or a sink at the corner point. These flows are presently known as Jeffery-Hamel flows. Rosenhead [7] was the first to give the complete set of solutions to the problem of flow in sectors. He gave a classification of flows depending on the opening angle 2α and the Reynolds number Re . For each pair of values of (α, Re) there exists an infinity of solutions to the Jeffery-Hamel problem. The majorities of these solutions will be of no practical importance as they will be highly unstable.

The qualitatively different solutions have been classified by Frankel [8] and the most common flows are referred to as II_1 , II_2 , IV_1 and V_1 . These may be seen sketched schematically in Figure 1.2.

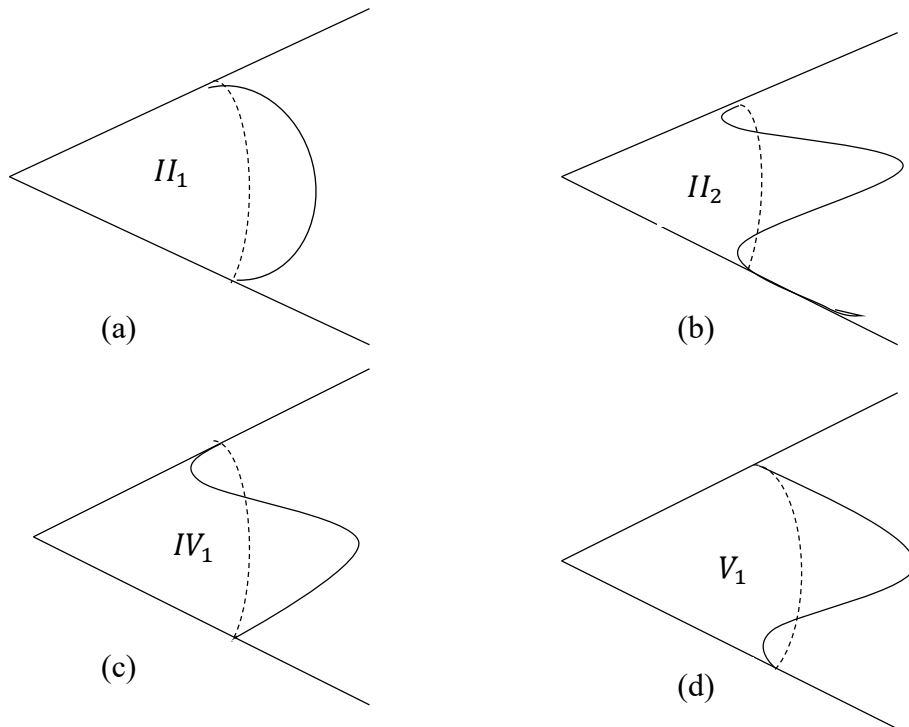


Figure 1.2: The Flow regimes II_1 , II_2 , IV_1 and V_1

The different types of Jeffery-Hamel flow exist in different regions of the (α, Re) plane. Frankel [8] gave solutions together with the analysis with bifurcations. It starts at some low Re solution and a fixed angle α , continues a solution to $Re > 0$ (net outflow) and $Re < 0$ (net inflow). However, the problem is non-linear and non-uniqueness of solutions at a fixed angle and Reynolds number is common. In this regard, one may be interested in those points in the $\alpha - Re$ plane that correspond to bifurcations of the Jeffery-Hamel states. These boundaries are shown schematically in Figure 1.3. Some of the properties that the solution possesses on the boundaries presented in Figure 1.3 are useful in this work.

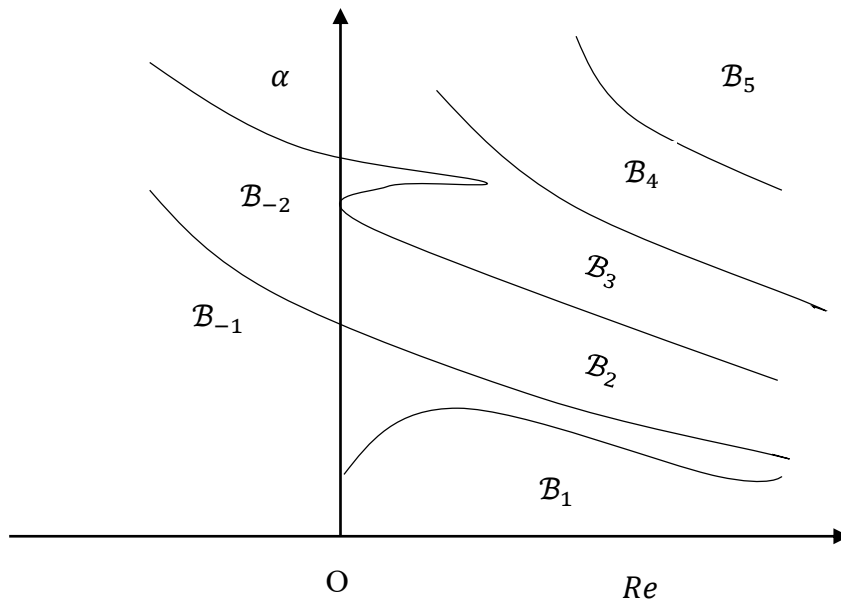


Figure 1.3: A Schematic diagram of the $\alpha - Re$ relation (Frankel [8])

The boundary B_1 and Re axis enclose a region in which solution type II_1 are available as denoted by Frankel [8]; these states corresponds to a symmetric flow with a single velocity maximum and no reverse flow. The most significant reverse flow solution is B_2 which exists between boundary B_2 and B_1 . The boundary between regions II_1 and II_2 is

given by the equation $Re = Re_2(\alpha)$ or $\alpha = \alpha_2(Re)$. As $\alpha \rightarrow 0$ then $Re_2(\alpha) \sim 4.712/\alpha$. Similarly, the boundary regions are denoted by $Re = Re_3(\alpha)$ or $\alpha = \alpha_3(Re)$ and as $\alpha \rightarrow 0$ then $Re_3(\alpha) \sim 5.461/\alpha$.

The Jeffery-Hamel solutions describe a flow in an idealized, infinite, domain rather than the practically relevant case of a system of finite streamwise extent. Various studies, both numerical and asymptotic, have attempted to relate Jeffery-Hamel solutions to the study of flow structure and stability in expanding channels of finite length. Banks *et al.* [9] addressed the spatial stability of symmetric Jeffery-Hamel flows by allowing for linearized perturbations suggested by Dean [10]. Their work reported that a loss of stability occurs at the pitchfork bifurcation boundary \mathcal{B}_2 . They computed the corresponding eigenmode, but only for small or zero Reynolds number for which the flow is nonlinear. The work of Goldshilk *et al.* [11] presented limited results at Reynolds numbers for which flow is nonlinear. Later Dennis *et al.* [12] performed a numerical study of the steady flow in a wedge for the ratios of outlet to inlet radius between 7 and 25. They examined the effect of imposing a small perturbation across either the inlet or the outlet to explore the relevance of Deans mode in a finite domain. They observed the loss of stability of symmetric base flow to antisymmetric perturbations but were unable to provide a critical Reynolds number, specifying only for that $\alpha = \pi/18$, the flow was stable for such perturbations for $Re = 50$ and was unstable for $Re = 100$. Numerical study of symmetry-broken solutions were located at Reynolds number greater than critical Reynolds number \widehat{Re}_c and the bifurcations is a supercritical pitchfork for finite domains.

Both Banks *et al.* [9] and Sobey *et al.* [13] identified the boundary \mathcal{B}_2 as the point at which the Jeffery-Hamel solutions provide a good description of the flow in an expanding channel. They performed numerical computations and experiments for a finite two-

dimensional channel, but only for an expansion ratio (the outlet width divided by inlet width) of less than or equal to three. In these short domains, a supercritical pitchfork bifurcation was observed to exist numerically and experimentally.

Hamadiche *et al.* [14] presented the results of calculations in a wedge of finite length, finding a neutral curve for temporal stability in good agreement with \mathcal{B}_2 for small α . Putkaradze *et al.* [15] examined the experimental study of the flow in a wedge angle 0.28 and radius ratio (η) approximately equal to 29. They confirmed that pure outflow solution is stable and that is always obtained for $Re < \widehat{Re}_c$. Tutty [16] investigated finite domain flows at Reynolds number close to \widehat{Re}_c and observed the existence of a steady solution, which at large distances from the inlet appeared to be spatially periodic (on the logarithm scale) in the radial coordinate. For values of Reynolds number greater than \widehat{Re}_c suggesting some form of instability of the symmetric Jeffery-Hamel solution. For Reynolds number less than the critical values ‘steady waves’ were only observed when the inlet geometry incorporated a sudden step extension. Tutty [16] interpreted the existence of the wave for Reynolds number less than Re_c the flow becomes unstable. Haines *et al.* [17] investigated the Jeffery-Hamel similarity solution in two-dimensional diverging channel and observed that symmetry-breaking pitchfork bifurcation for $Re = 94.72$.

1.2 Stability Analysis for Systems

In a dynamic system, only the solutions of linear systems may be found explicitly. The problem is that in general real-life problems may be modeled by nonlinear systems. The main idea is to approximate a nonlinear system by a linear one (around the equilibrium point). Of course, the behavior of the solutions of the linear system will be the same as the nonlinear one.

Consider a nonlinear differential equation

$$x'(t) = f(x(t), u(t))$$

where f is a function mapping $\mathfrak{R}^n \times \mathfrak{R}^m \rightarrow \mathfrak{R}^n$. A point \bar{x} is called an equilibrium point if there is a specific $\bar{u} \in \mathfrak{R}^m$ such that

$$f(x(t), u(t)) = 0$$

Suppose \bar{x} is an equilibrium point (with the input \bar{u}). Consider the initial condition $x(0) = \bar{x}$, applying the input $u(t) = \bar{u}$ for all $t \geq t_0$, then resulting solutions $x(t)$ satisfies

$$x(t) = \bar{x},$$

For all $t \geq t_0$. That is why it is called an equilibrium point or solution

Consider two-dimensional nonlinear system

$$x' = f(x, y),$$

$$y' = g(x, y),$$

And suppose that (\bar{x}, \bar{y}) is a steady state (equilibrium point), i.e.,

$$f(\bar{x}, \bar{y}) = 0 \quad \text{and} \quad g(\bar{x}, \bar{y}) = 0$$

Now let's consider small perturbation from the steady state (\bar{x}, \bar{y})

$$x = \bar{x} + u,$$

$$y = \bar{y} + v,$$

where u and v are understood to be small as $u \ll 1$ and $v \ll 1$. If it moves away, it is called unstable equilibrium point, if it moves towards the equilibrium point, then it is called stable equilibrium point. As in scalar equations, by expanding the Taylor's series for $f(x, y)$ and $g(x, y)$;

$$\begin{aligned} u' &= x' = f(x, y) \\ &= f(\bar{x} + u, \bar{y} + v) \\ &= f(\bar{x}, \bar{y}) + f_x(\bar{x}, \bar{y})u + f_y(\bar{x}, \bar{y})v + \text{higher order terms} \dots \end{aligned}$$

$$= f_x(\bar{x}, \bar{y})u + f_y(\bar{x}, \bar{y})v + \text{higher order terms} \dots\dots$$

Similarly,

$$\begin{aligned} v' &= y' = g(x, y) \\ &= g(\bar{x} + u, \bar{y} + v) \\ &= g(\bar{x}, \bar{y}) + g_x(\bar{x}, \bar{y})u + g_y(\bar{x}, \bar{y})v + \text{higher order terms} \dots\dots\dots \\ &= g_x(\bar{x}, \bar{y})u + g_y(\bar{x}, \bar{y})v + \text{higher order terms} \dots\dots\dots \end{aligned}$$

Since u and v are assumed to be small, the higher orders terms are extremely small, we can neglect the higher order terms and obtain the following linear systems of equations governing the evolution of perturbations u and v ,

$$\begin{bmatrix} u' \\ v' \end{bmatrix} = \begin{bmatrix} f_x(\bar{x}, \bar{y}) & f_y(\bar{x}, \bar{y}) \\ g_x(\bar{x}, \bar{y}) & g_y(\bar{x}, \bar{y}) \end{bmatrix} \begin{bmatrix} u \\ v \end{bmatrix}$$

Where the matrix $J = \begin{bmatrix} f_x & f_y \\ g_x & g_y \end{bmatrix}$ is called the Jacobian matrix of the nonlinear system.

The above linear system for u and v has the trivial steady state $(u, v) = (0, 0)$ and the stability of trivial steady state is determined by the eigenvalues of the Jacobian matrix, as follows:

- **Asymptotically stable:** A critical point is asymptotically stable if all eigenvalue of the Jacobian matrix are negative, or have negative real parts.
- **Unstable:** A critical point is unstable if at least one eigenvalue of the Jacobian matrix has positive or has positive real parts.
- **Stable (neutrally stable):** Each trajectory moves about the critical point within a finite range of distance.
- **Hyperbolic point:** The equilibrium is said to be hyperbolic if all eigenvalues of the Jacobian Matrix have non-zero real parts. Hyperbolic equilibria are robust (i.e. the system is structurally stable). Small perturbations of order do not change

qualitatively the phase portrait near equilibria. Moreover, the local phase portrait of a hyperbolic equilibrium of a nonlinear system is equivalent to its linearization.

- **Non-hyperbolic point:** If at least one eigenvalue of the Jacobian matrix is zero or has a zero real part, then the equilibrium is said to be non-hyperbolic. Non-hyperbolic equilibrium is not robust. Small perturbations can result in a local bifurcation of a non-hyperbolic equilibrium, i.e. it can change stability.

Example 1.1: Consider the following nonlinear system

$$\dot{x}(t) = y(t)[x(t) - y(t)]$$

$$\dot{y}(t) = x(t)[2 - y(t)]$$

The equilibria are the points $(\hat{x}, \hat{y}) = (0, 0)$ and $(\hat{x}, \hat{y}) = (1, 2)$ and the Jacobian matrix is

$$J = \begin{bmatrix} y & x - 1 \\ 2 - y & -x \end{bmatrix}$$

computed the Jacobian matrix at the equilibrium point $(0, 0)$ where $J(0, 0) = \begin{bmatrix} 0 & -1 \\ 2 & 0 \end{bmatrix}$

which implies that the eigenvalues are purely imaginary.

$$\lambda_{1,2} = \pm\sqrt{2}i$$

By solving the characteristic equation

$$\det(J - \lambda I) = 0$$

Since the system is non hyperbolic the linearized system can not tell about the stability.

For the equilibrium point $(1, 2)$, the jacobian matrix $J(1,2) = \begin{bmatrix} 2 & 0 \\ 0 & -1 \end{bmatrix}$ thus the point is

locally unstable as $\lambda_1 = 1$ or $\lambda_2 = -1$. Since it is a hyperbolic equilibrium point, the stability of Fixed point is the same as linearized system. So it is unstable.

1.3 Basic Concepts of Bifurcation Analysis

Bifurcation Analysis is a powerful method for studying the steady-state non-linear dynamics of the system. Performing a bifurcation analysis is often a powerful way to analyze the properties of a system. This thesis, Jeffery-Hamel flow is investigated which is a non-linear problem in fluid dynamics. Solutions to a non-linear problems often involve one or several parameters. As the parameter varies, so does the solution set. A bifurcation occurs when a small smooth change made to the values of the parameters (the bifurcation parameters) of a system causes a sudden ‘qualitative’ or topological change in its behavior. Bifurcation has two types;

- **Local bifurcations:** Local bifurcations can be analyzed entirely through changes in the local stability properties of equilibria, periodic orbit or other invariant sets as parameters cross through critical thresholds.
- **Global bifurcations:** Global bifurcations which often occur in larger invariant sets of the system “collide” with each other, or with equilibria of the system. They can not be detected purely by a stability analysis of equilibria.

A detailed discussion can be found in Kuznetsov [18], Strogatz [19], and wiggins [20]. Some useful local bifurcations analysis of the present study are discussed below.

1.3.1 The Pitchfork Bifurcation

In pitchfork bifurcation, one family of fixed points transfers its stability properties to two families after or before the bifurcation point. If this occurs after the bifurcation point, then the pitchfork bifurcation is called supercritical. Similarly, a pitchfork bifurcation is called subcritical if the non-trivial fixed point occurs for values of the parameter lower than the bifurcation value. In other words, the cases in which emerging nontrivial equilibria are called supercritical otherwise these equilibria are called subcritical.

Consider the dynamical system

$$x' = ax - bx^3 \text{ for } a, b \text{ are real .}$$

a and b are external control parameters. Steady states, for which $x' = 0$ are as follows

$$\begin{aligned} x = \bar{x}_1 &= 0, \forall a, b, \\ x = \bar{x}_2 &= -\sqrt{a/b}, \text{ for } a/b > 0 \\ x = \bar{x}_3 &= \sqrt{a/b}, \text{ for } a/b > 0 \end{aligned}$$

The equilibrium points \bar{x}_2 and \bar{x}_3 only exist when $a > 0$ if $b > 0$ and for $a < 0$ if $b < 0$.

Now examine the linear stability of these steady state in turn. First we write the perturbation for $\bar{x}_1 = 0$,

$$x = \bar{x}_1 + \epsilon$$

That yields the linearized equation

$$\frac{d\epsilon}{dt} = a\epsilon,$$

With the new solution

$$e(t) = Ae^{at}$$

So we see that

The state $\bar{x}_1 = 0$ is linearly unstable if $a > 0$,

The state $\bar{x}_2 = 0$ is linearly stable if $a < 0$

For the states $x = \bar{x}_2$ and $x = \bar{x}_3$, setting

$$\begin{aligned} \bar{x} &= \pm\sqrt{a/b} + \epsilon, \\ \frac{d\epsilon}{dt} &= a\epsilon - 3bx^{-2}\epsilon \end{aligned}$$

With the solution

$$e(t) = A e^{ct} \text{ where } c = -2a$$

That is the obvious that

The state \bar{x}_2 and \bar{x}_3 are linearly stable if $a > 0$

The state \bar{x}_2 and \bar{x}_3 are linearly unstable if $a < 0$

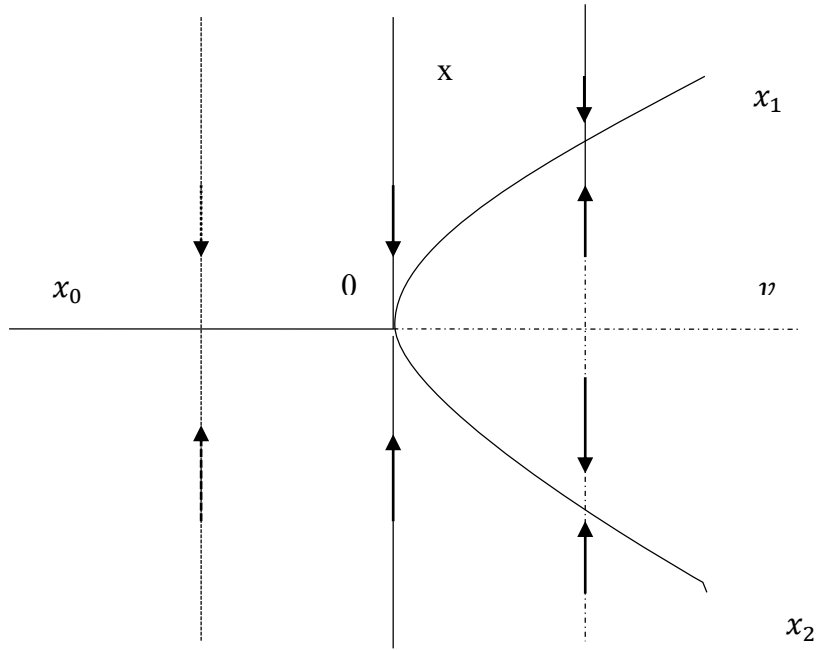


Figure 1.4: Diagram corresponding to pitchfork bifurcation

1.3.2 Hopf Bifurcation

A Hopf bifurcation is a local bifurcation in which a fixed point of a dynamical system loses stability as a pair of complex conjugate eigenvalues of linearization around the fixed point cross the imaginary axis of the complex plane. Consider the two dimensional system

$$\frac{dx}{dt} = f(x, y, \tau)$$

$$\frac{dy}{dt} = g(x, y, \tau)$$

where τ is the parameter and suppose that $(x(\tau), y(\tau))$ is the equilibrium point and $\alpha(\tau) \pm i\beta(\tau)$ are the eigenvalues of the Jacobian matrix which is evaluated at the equilibrium point. First the system is transformed so that the equilibrium is at origin and

the parameter τ at $\tau^* = 0$ gives purely imaginary eigenvalues. Above system is re-written as follows;

$$\frac{dx}{dt} = a_{11}(\tau)x + a_{12}(\tau)y + f_1(x, y, \tau)$$

$$\frac{dy}{dt} = a_{21}(\tau)x + a_{22}(\tau)y + g_1(x, y, \tau)$$

The linearization of the system about the origin is given by $\frac{dX}{dt} = J(\tau)X$, where $X = \begin{bmatrix} x \\ y \end{bmatrix}$ and

$$J(\tau) = \begin{bmatrix} a_{11}(\tau) & a_{12}(\tau) \\ a_{21}(\tau) & a_{22}(\tau) \end{bmatrix}$$

is the Jacobian Matrix evaluated at the origin. The Hopf bifurcation is called supercritical if the equilibrium point $(0, 0)$ is asymptotically stable when $\tau = 0$ and it is called subcritical if the equilibrium point $(0, 0)$ is negatively asymptotically stable (as $t \rightarrow -\infty$) when $\tau = 0$. In a supercritical Hopf bifurcation the limit cycle grows out of the equilibrium point. In a subcritical Hopf bifurcation, there is an unstable limit cycle surrounding the equilibrium point, and a stable limit cycle surrounding that.

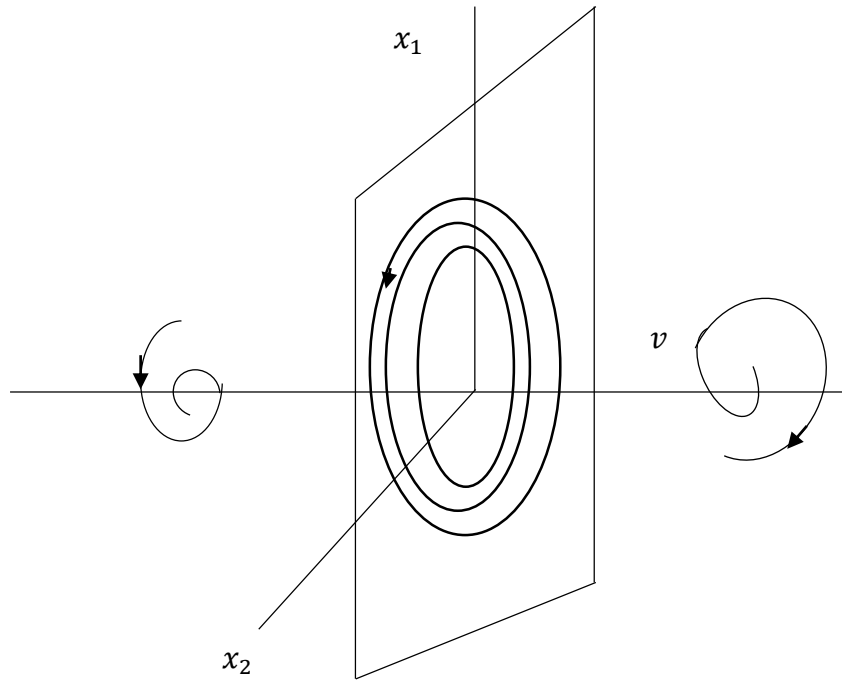


Figure 1.5: Diagram corresponding to Hopf bifurcation

1.4 Objectives of the Present Work

This thesis is concerned with the study of computer-based approximation techniques which are of Hermite-Padé class and the Finite Element Method. The present study is a stability analysis of the Jeffery-Hamel solution and its relation to flow in a diverging channel. Numerical results are presented for the two-dimensional flow in a wedge of separation angle 2α , bounded by circular arcs at the inlet/outlet and for a net radial outflow of the fluid.

The purpose of the current work is as follows:

- To study the evolution of Jeffery-Hamel flow in a diverging channel of finite (but large) streamwise extent.
- To implement the Finite Element Method and Hermite-Padé approximation Method for solving the problems of steady viscous fluid flow in sectors.

- To examine the stability behavior of the solution with the effect of Reynolds number, angle, and effect of radius ratio.

1.5 Organization of the Thesis

The thesis contains five Chapters. In this Chapter, a brief introduction is presented with a literature review. The remaining Chapter organized as follows

- Chapter 2 presents the computational procedure of the problem.
- Chapter 3 a detailed mathematical modelling of the problem.
- Chapter 4 results, as well as discussion, are presented.
- Chapter 5 summarized the problem and give some ideas for future work.

CHAPTER 2

COMPUTATIONAL TECHNIQUE

Computational Fluid Dynamics (CFD) technique and Approximant's Power Series technique are two popular techniques employed to analyze fluid flow problems in complex geometries. Computational Fluid Dynamics is the branch of fluid dynamics providing cost-effective means of simulating real flows by the numerical way and so amenable to solve the governing equations. It replaces the governing partial differential equations with systems of algebraic equations that are much easier to solve using computers. It also can allow for the testing of conditions that are not possible or extremely difficult to measure experimentally and are not controllable to analytic solutions.

Computational Fluid dynamics use in numerical investigations and data structures to analyze and solve problems involving fluid flows. CFD is applied to a wide range of research and engineer's problem in many fields of study and industries including aerodynamics and aerospace analysis weather simulation, natural science and environmental engineering, industrial system of design and analysis, biological engineering, and fluid flows. Therefore CFD codes need that can make physically realistic results with good quality accuracy in simulations with finite grids. Contained within the broad field of computational fluid dynamics are activities that cover the range from automation of well-established engineering design methods to the use of detailed solutions of the Navier-Stokes equations as substitutes for experimental research into the nature of complex flows. More details are available in Cengul *et al.* [21] and Chung [22].

In Approximant's Power Series technique, Hermite-Padé approximant is the best approximation of a function by a rational function of given order-under this technique, the approximant power series agrees with the power series of the function it is

approximating. The Hermite-Padé approximant often gives a better approximation of the function than truncating its Taylor series and it still works where the Taylor series does not converge. For these reasons, Hermite-Padé are used extensively in fluid flow problem calculation.

2.1 Numerical Solution Method of Computational Fluid Dynamics

Several elements of numerical solution methods are available in Ferziger and Perić [23] here only the main steps will be demonstrated following.

2.1.1 Mathematical Model

The primary task of any numerical solution method we have to provide a mathematical model, i.e. the set of partial differential equations and its related boundary conditions. A solution method is usually planned for a particular set of equations. Trying to procedure a general-purpose solution method, i.e. one which is applied to all flows, is impractical, is not impossible and as with most general-purpose tools, they are usually not optimum for any one application.

2.1.2 Discretization Method

After choosing the mathematical model, one has to select a suitable discretization method, i.e. a method of approximation the differential equations by a system of algebraic equations for the variable at some set of discrete locations in space and time.

2.1.3 Numerical Grid

The next step is to select a numerical grid that defines the discrete locations, at which the variable is to be calculated. It is essentially a discrete representation of the geometric domain on which the problem is to be solved. It divides the solution domain into a finite

number of sub-domains such as elements, control volumes, etc. Some of the options available are structural (regular) grid, bloc structured grid, unstructured grid, etc.

2.1.4 Finite Approximations

Following the choice of grid type, one has to choose the approximations to be used in the discretization process. Approximations for the derivatives at the grid points have to be selected in a finite difference method. In a finite volume method, one has to select the methods of approximating surface and volume integrals. In a finite element method, one has to choose the functions and weighted functions.

2.1.5 Solution Technique

Discretization yields a large system of non-linear algebraic equations. The method of a solution depends on the type of problem. For unsteady flows, the method based on those used for initial value problems for the ordinary differential equation is used. Since the equations are non-linear, an iteration scheme is used to solve them. The choice of solver depends on the grid type and the number of nodes involved in each algebraic equation.

2.2 Discretization Approaches

One is to consider numerical discretization to solve a mathematical model of physical phenomena. This means that each component of the differential equations is transformed into a “numerical analogue” which can be represented in the computer and then processed by a computer program, built on some algorithm. There are many different methodologies that were introduced for this purpose in the past and the development still continues. Some special methods are

- Finite Difference Method
- Finite Volume Method

- Finite Element Method
- Boundary Element Method
- Boundary Volume Method

In the present numerical computation, Galerkin Finite Element Method (FEM) has been used. A detailed discussion of this method is available in Ferziger and Perić [23] and Dechaumphai [24].

2.2.1 Finite Element Method

The Finite Element Method (FEM) has developed into a key, indispensable technology in the modelling and simulation of advanced engineering systems in various fields like housing, transportation, communication and so on. In building such advanced engineering systems, engineers and designers go through a sophisticated process of modelling, simulation, visualization, analysis, designing, and so on.

The FEM is a numerical method seeking an approximated solution of the distribution of field variables in the problem domain that is difficult to obtain analytically. This computational method in which a given domain is represented as a collection of simple domains, called finite elements, for which it is possible to systematically construct the approximation functions needed in the solution of partial differential equations by the weighted residual method. The computational domains with irregular geometries by a collection of finite elements make the method a valuable practical tool for the solution of boundary value problems arising in various fields of engineering. The approximation functions, which satisfy the governing equations and boundary conditions, are often constructed using the ideas from interpolation theory. Approximating functions in Finite Elements are determined in terms of nodal values of a physical field, which is required. A continuous physical problem is transformed into a discretized Finite Element problem

with unknown nodal values. Values inside Finite Elements can be recovered using nodal values. The major steps involved in Finite Element analysis of a typical problem are:

- Weighted-integral or weak formulation of the differential equation to be analyzed.
- Development of the Finite Element Model of the problem using its weighted-integral or weak form.
- Assembly of Finite Elements to obtain the global system of algebraic equations.
- Impositions of boundary conditions.
- Solution of equations.
- Post-computation of solution and quantities of interest.

2.2.2 Mesh Generation

The first step is to discretize the domain into non-overlapping elements or sub-regions. The Finite Element Method allows a variety of element shapes, for example, triangles, quadrilaterals in two dimensions, and tetrahedral, hexahedral, and prisms in three dimensions. Each element is formed by the connection of nodes, with the number of nodes in an element. The number of nodes in each element does not depend only on the number of corner points in the element, but also on the type of the element interpolation function. A detailed discussion of this available in Reddy and Gartling [25] and Sayma [26].

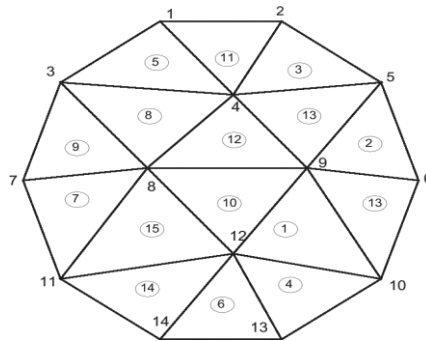


Figure 2.1: A typical two-dimensional Finite Element mesh (Reddy and Gartling [25])

2.2.3 Computational Procedure of Finite Element Formulation

Viscous incompressible thermal flows have been the subject of our investigation. The problem is non-linear partial differential equations, which are difficult to solve especially with complicated geometries and boundary conditions.

The algorithm of computational procedure was originally put forward by the iterative Newton-Raphson algorithm; the discrete forms of the continuity, momentum equations are solved to find out the value of the related parameter. It is essential to guess the initial values of the variable. Then the numerical solutions of the variables are obtained while the convergent criterion is fulfilled. The simple algorithm is shown by the flow chart below:

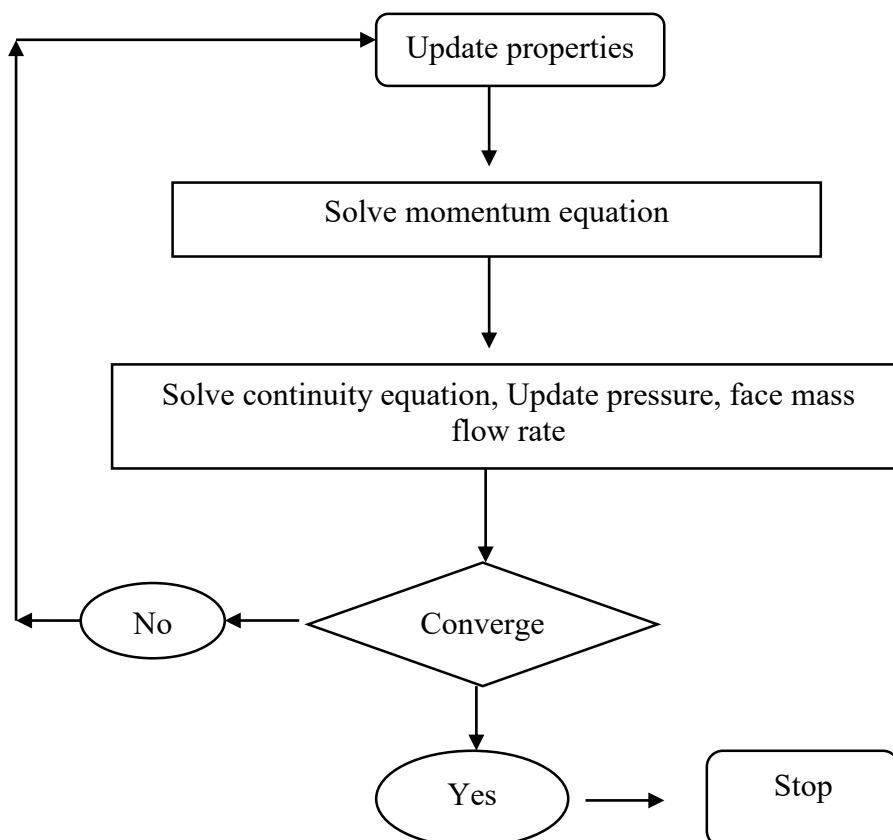


Figure 2.2: Flow chart of computational procedure

2.3 Solution Technique of Hermite-Padé Approximant Method

In 1893, Hermite and Padé introduced Hermite-Padé class. In its most general form, this class is concerned with the simultaneous approximation of several independent series. Here only several steps of series analysis are discussed; detailed discussion of this method are available in Baker *et al.* [27], Mankinde [28] and Khan [29].

Firstly describing the Hermite-Padé class from its point of view.

Let $d \in N$ and let $d + 1$ power series $U_0(x), U_1(x), \dots, U_d(x)$ are given. We say that $(d + 1)$ tuple of polynomials

$$P_N^{[0]}, P_N^{[1]}, \dots, P_N^{[d]}$$

$$\text{where } \deg P_N^{[0]} + \deg P_N^{[1]} + \dots + \deg P_N^{[d]} + d = N$$

is a Hermite-Padé form of these series if

$$\sum_{i=0}^d P_N^{[i]}(x)U_i(x) = O(x^N) \text{ as } x \rightarrow 0$$

Here $U_0(x), U_1(x), \dots, U_d(x)$ may be independent series or different form of a unique series. Polynomials of $P_N^{[i]}$ need to find out that satisfy the above equation. These polynomials are completely determined by their coefficient. So, the total number of unknown in above equation is

$$\sum_{i=0}^d \deg P_N^{[i]} + d + 1 = N + 1$$

Expanding the left side of equation in $\sum_{i=0}^d P_N^{[i]}(x)U_i(x) = O(x^N) \text{ as } x \rightarrow 0$ powers of x and equating the first N equations of the system equal to zero, a system of

linear homogeneous equations are found. To calculate the coefficients of the Hermite-Padé polynomials we required some sort of normalizations, such as

$$P_N^{[i]}(0) = 1 \text{ for some } 0 \leq i \leq d$$

It is important to emphasize that the only input required for the calculation of Hermite-Padé polynomials are the first N coefficient of the series U_0, \dots, U_d . The equations $P_N^{[i]}(0) = 1$ for some $0 \leq i \leq d$; simply ensures that the co-efficient matrix associated with the system is square. One way to construct Hermite-Padé polynomials is to solve the system of linear equations by any standard method such as Gaussian elimination or Gauss-Jordan elimination.

In the next Chapter, the formulation of Jeffery-Hamel Flow in a Diverging Channel will be discussed.

CHAPTER 3

MATHEMATICAL MODELLING

3.1 General

The primary task of any numerical method is to set mathematical formulation, i.e. to set up generalized governing equations and boundary conditions. A solution method is usually designed to solve a particular set of equations. These governing equations are generally based on the conservation laws of mass, momentum, and energy equations.

3.2 Physical Configurations

The considered geometry of Jeffery-Hamel Flow in a Diverging Channel is a finite section of wedge bounded by circular arc at inlet and outlet of constant radius as depicted in Figure 3.1. The numerical problem is formulated in terms of polar co-ordinate (r, θ) centred on the apex of the wedge with corresponding velocities (u, v) and pressure p . Two walls separated by a fixed angle 2α for which $\widehat{R}_i \leq r \leq \widehat{R}_o$. The circular arcs at \widehat{R}_i and \widehat{R}_o are referred to as the inlet and outlet boundaries respectively. After non-dimensionalization, the size of the domain will be parameterized by the radius ratio $\eta =$

$$\frac{\widehat{R}_o}{\widehat{R}_i}$$

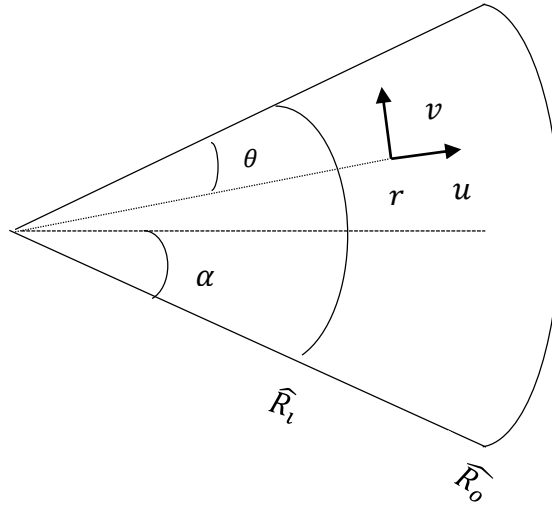


Figure 3.1: Geometry for Jeffery-Hamel flow

3.3 Mathematical Formulation

The several steps of the mathematical formulation for the above physical configurations are shown as follows

3.3.1 Governing equations

The generalized governing equations are considered the flow of an incompressible Viscous fluid due to a source that is present at the intersection of two rigid non-parallel walls, the angle between walls is 2α . Flow is assumed to be symmetric and purely radial. These assumptions mean that the velocity field is of the form $\mathbf{V} = [u_r, u_\theta]$ where u_r is a function of both r and θ .

The equations of motions for the flow are given as

$$\nabla \cdot \mathbf{V} = 0, \quad (3.1)$$

$$\rho \left[\frac{\partial \mathbf{V}}{\partial t} + (\mathbf{V} \cdot \nabla) \mathbf{V} \right] = -\nabla P + \mu \nabla^2 \mathbf{V} \quad (3.2)$$

Where V, ρ, μ, P is the velocity vector, constant density, dynamic viscosity, and pressure respectively. Also ∇^2 is the Laplacian operator given by

$$\nabla^2 = \frac{\partial^2}{\partial r^2} + \frac{1}{r} \frac{\partial}{\partial r} + \frac{1}{r^2} \frac{\partial^2}{\partial \theta^2}$$

Incompressible continuity equation:

$$\frac{1}{r} \frac{\partial(ru_r)}{\partial r} + \frac{1}{r} \frac{\partial(u_\theta)}{\partial \theta} = 0 \quad (3.3)$$

Momentum equation for r direction

$$\rho \left(\frac{\partial u_r}{\partial t} + u_r \frac{\partial u_r}{\partial r} + \frac{u_\theta}{r} \frac{\partial u_r}{\partial \theta} - \frac{u_\theta^2}{r} \right) = F_r - \frac{\partial p}{\partial r} + \mu \left[\frac{\partial}{\partial r} \left(\frac{1}{r} \frac{\partial}{\partial r} (ru_r) \right) + \frac{1}{r^2} \frac{\partial^2 u_r}{\partial \theta^2} - \frac{2}{r^2} \frac{\partial u_\theta}{\partial \theta} \right] \quad (3.4)$$

$$\text{Here, } \frac{\partial}{\partial r} \left(\frac{1}{r} \frac{\partial}{\partial r} (ru_r) \right) = \frac{\partial}{\partial r} \left(\frac{\partial u_r}{\partial r} + \frac{1}{r} u_r \right)$$

$$\frac{\partial}{\partial r} \left(\frac{1}{r} \frac{\partial}{\partial r} (ru_r) \right) = \frac{\partial^2 u_r}{\partial r^2} + \frac{1}{r} \frac{\partial u_r}{\partial r} + u_r \frac{\partial}{\partial r} \left(\frac{1}{r} \right)$$

$$\frac{\partial}{\partial r} \left(\frac{1}{r} \frac{\partial}{\partial r} (ru_r) \right) = \frac{\partial^2 u_r}{\partial r^2} + \frac{1}{r} \frac{\partial u_r}{\partial r} - \frac{u_r}{r^2}$$

Now the equation (3.4) becomes

$$\rho \left(\frac{\partial u_r}{\partial t} + u_r \frac{\partial u_r}{\partial r} + \frac{u_\theta}{r} \frac{\partial u_r}{\partial \theta} - \frac{u_\theta^2}{r} \right) = F_r - \frac{\partial p}{\partial r} + \mu \left[\frac{\partial^2 u_r}{\partial r^2} + \frac{1}{r} \frac{\partial u_r}{\partial r} - \frac{u_r}{r^2} + \frac{1}{r^2} \frac{\partial^2 u_r}{\partial \theta^2} - \frac{2}{r^2} \frac{\partial u_\theta}{\partial \theta} \right] \quad (3.5)$$

Momentum equation for θ direction:

$$\rho \left(\frac{\partial u_\theta}{\partial t} + u_r \frac{\partial u_\theta}{\partial r} + \frac{u_\theta}{r} \frac{\partial u_\theta}{\partial \theta} + \frac{u_r u_\theta}{r} \right) = F_\theta - \frac{1}{r} \frac{\partial p}{\partial \theta} + \mu \left[\frac{\partial}{\partial r} \left(\frac{1}{r} \frac{\partial}{\partial r} (ru_\theta) \right) + \frac{1}{r^2} \frac{\partial^2 u_\theta}{\partial \theta^2} + \frac{2}{r^2} \frac{\partial u_r}{\partial \theta} \right] \quad (3.6)$$

$$\frac{\partial}{\partial r} \left(\frac{1}{r} \frac{\partial}{\partial r} (ru_\theta) \right) = \frac{\partial^2 u_\theta}{\partial r^2} + \frac{1}{r} \frac{\partial u_\theta}{\partial r} - \frac{u_\theta}{r^2}$$

So the equation (3.6) becomes

$$\begin{aligned} & \rho \left(\frac{\partial u_\theta}{\partial t} + u_r \frac{\partial u_\theta}{\partial r} + \frac{u_\theta}{r} \frac{\partial u_\theta}{\partial \theta} + \frac{u_r u_\theta}{r} \right) \\ & = F_\theta - \frac{1}{r} \frac{\partial p}{\partial \theta} + \mu \left[\frac{\partial^2 u_\theta}{\partial r^2} + \frac{1}{r} \frac{\partial u_\theta}{\partial r} - \frac{u_\theta}{r^2} + \frac{1}{r^2} \frac{\partial^2 u_\theta}{\partial \theta^2} + \frac{2}{r^2} \frac{\partial u_r}{\partial \theta} \right] \end{aligned} \quad (3.7)$$

It is assumed that the flow is steady and purely radial ($u_\theta = 0$) then the incompressible Navier-Stokes equations (3.3), (3.5), (3.7) in absence of body force ($F_r = F_\theta = 0$) simply reduces to;

$$\frac{1}{r} \frac{\partial}{\partial r} (ru_r) = 0 \quad (3.8)$$

$$u_r \frac{\partial u_r}{\partial r} = -\frac{1}{\rho} \frac{\partial p}{\partial r} + \nu \left(\frac{\partial^2 u_r}{\partial r^2} + \frac{1}{r} \frac{\partial u_r}{\partial r^2} - \frac{u_r}{r^2} + \frac{1}{r^2} \frac{\partial^2 u_r}{\partial \theta^2} \right) \quad (3.9)$$

$$-\frac{1}{\rho} \frac{\partial p}{\partial \theta} + \frac{2\nu}{r} \frac{\partial u_r}{\partial \theta} = 0 \quad (3.10)$$

With the boundary conditions are no slip on the solid walls ($u_r(r, \pm\alpha) = 0$) and symmetry about the centerline ($\theta = 0$) of the channel.

3.3.2 Dimensional Analysis

The solution of equation (3.8) is particularly simple and inspires to form the non-dimensional solution of the problem. Integrating (3.8) gives:

$$u_r = \frac{g(\theta)}{r} \quad (3.11)$$

From (3.9)

$$\frac{g(\theta)}{r} \frac{\partial}{\partial r} \left(\frac{g(\theta)}{r} \right) = -\frac{1}{\rho} \frac{\partial p}{\partial r} + \nu \left[\frac{\partial^2}{\partial r^2} \left(\frac{g(\theta)}{r} \right) + \frac{1}{r} \frac{\partial}{\partial r} \left(\frac{g(\theta)}{r} \right) - \frac{1}{r^2} \frac{g(\theta)}{r} + \frac{1}{r^2} \frac{\partial^2}{\partial \theta^2} \left(\frac{g(\theta)}{r} \right) \right] \quad (3.12)$$

$$\frac{\partial}{\partial r} \left(\frac{g(\theta)}{r} \right) = -g(\theta) \frac{1}{r^2}$$

$$\frac{\partial^2}{\partial r^2} \left(\frac{g(\theta)}{r} \right) = \frac{2g(\theta)}{r^3}$$

$$\frac{\partial}{\partial \theta} (g(\theta)) = g'(\theta)$$

$$\frac{\partial^2}{\partial \theta^2} (g(\theta)) = g''(\theta)$$

Now from equation (3.12)

$$\begin{aligned} \frac{g(\theta)}{r} \left(-g(\theta) \frac{1}{r^2} \right) &= -\frac{1}{\rho} \frac{\partial p}{\partial r} + v \left[\frac{2g(\theta)}{r^3} + \frac{1}{r} \left(-g(\theta) \frac{1}{r^2} \right) - \frac{1}{r^2} \left(\frac{g(\theta)}{r} \right) + \frac{1}{r^2} \frac{1}{r} (g''(\theta)) \right] \\ -\frac{g^2(\theta)}{r^3} &= -\frac{1}{\rho} \frac{\partial p}{\partial r} + v \left[\frac{2g(\theta)}{r^3} - \frac{2g(\theta)}{r^3} + \frac{g''(\theta)}{r^3} \right] \end{aligned} \quad (3.13)$$

$$-\frac{g^2(\theta)}{r^3} = -\frac{1}{\rho} \frac{\partial p}{\partial r} + v \quad (3.14)$$

From equation (3.10)

$$\begin{aligned} -\frac{1}{\rho} \frac{\partial p}{\partial \theta} + \frac{2v}{r^2} \frac{1}{\partial \theta} \left(\frac{g(\theta)}{r} \right) &= 0 \\ -\frac{1}{\rho} \frac{\partial p}{\partial \theta} + \frac{2v}{r^3} g'(\theta) &= 0 \end{aligned} \quad (3.15)$$

Now differentiating equation (3.14) with respect to θ and equation (3.15) with respect to r , we get

$$-\frac{2}{r^3} g(\theta) g''(\theta) = -\frac{1}{\rho} \frac{\partial^2 p}{\partial \theta \partial r} + v \left[\frac{1}{r^3} g'''(\theta) \right] \quad (3.16)$$

$$\frac{1}{\rho} \frac{\partial^2 p}{\partial \theta \partial r} = \frac{4v}{r^3} g'(\theta) \quad (3.17)$$

Equation (3.16) becomes

$$\begin{aligned} -\frac{2}{r^3} g(\theta) g''(\theta) &= \frac{4v}{r^3} g'(\theta) + v \left[\frac{1}{r^3} g'''(\theta) \right] \\ v g'''(\theta) + 2g(\theta) g'(\theta) + 4v g'(\theta) &= 0 \end{aligned} \quad (3.18)$$

Dimensionless parameter are defined as follow:

$$\phi = \frac{\theta}{\alpha}, \quad G(\phi) = \frac{g(\theta)}{U_{max} r \alpha} \quad (3.19)$$

where U_{max} is a centerline velocity.

Then equation (3.18) becomes

$$G'''(\phi) + 2\alpha Re G(\phi)G'(\phi) + 4\alpha^2 G'(\phi) = 0 \quad (3.20)$$

Let $\psi = \psi(r, \theta)$ be the stream function , then

$$\frac{\partial \psi}{\partial \theta} = ur, \quad \frac{\partial \psi}{\partial r} = 0 \quad (3.21)$$

Jeffery-Hamel form of the stream function ψ is

$$\psi(r, \theta) = QG(\phi) \quad (3.22)$$

Where Q is the volumetric flow rate through the channel is defined by

$$Q = \int_{-\alpha}^{\alpha} ur d\theta$$

Then the nonlinear differential equation for stream function $G(\phi)$ satisfies

$$G'''' + 2\alpha Re G'G'' + 4\alpha^2 G'' = 0 \quad (3.23)$$

Where primes indicate differentiation with respect to ϕ and $Re = \frac{Q}{\nu}$ is Reynolds number

The appropriate boundary conditions are

$$G(\pm 1) = \pm \frac{1}{2}, \quad G'(\pm 1) = 0 \quad (3.24)$$

Describing no slip and no penetration at the wedge walls.

Although the system (3.23) and (3.24) is known to have an infinite number of solutions for any value of the Reynolds number, the most concerning solutions are found by continuous variation from the Stokes solution.

3.4 Numerical Analysis

The governing equations along with the boundary conditions are solved numerically employing the Finite Element Method and Hermite-Padé Approximant Method discussed below.

3.4.1 Mathematical Formulation for Finite Element Method

We solve the resulting dimensionless form of the Navier-Stokes equations (3.20) using a Finite-Element Method. The Finite-domain problem is set up by non-dimensionalized in terms of the inlet constant radial volume flux Q and the outlet radius \widehat{R}_0 . The relevant velocity scale is then $U = Q/\widehat{R}_0$ so the dimensionless radial co-ordinate, velocity and pressure are

$$\hat{r} = \frac{r}{\widehat{R}_0}, \quad \hat{u} = \frac{u}{U}, \quad \hat{p} = \frac{\widehat{R}_0}{U\rho\nu} p$$

Where a hat indicates the corresponding dimensionless variable.

The parameter space for the computational problem is spanned by

$$\alpha, \quad Re = \frac{Q}{\nu}, \quad \eta = \frac{\widehat{R}_0}{\widehat{R}_i}$$

which are the wedge half-angle, a Reynolds number and the outlet/inlet radius ratio. The computational mesh is rectangular in the co-ordinate r and ϕ and comprises N_r elements in the radial direction and N_ϕ elements in the azimuthal direction. Initial mesh nodes are spaced logarithmically in the radial direction in order to minimize the error associated with resolving the inverse radius scaling of the Jeffery-Hamel similarity solution, however, the initial azimuthal spacing is generally uniform. To better resolve rapid

adjustments caused by the outlet boundary conditions, an outlet region with smaller radial spacing between the nodes was incorporated into the initial mesh structure.

The Finite-Element library FEM Multiphysics solver with MATLAB interface used to assemble and solve the system of algebraic equations associated with a weak form of the Navier-Stokes equations in plane polar coordinates on the finite domain.

3.4.1.1 Variation of Inlet Condition

In our Finite-element formulation, The implied, so-called natural, boundary condition is for the flow to be ‘pseudo-traction free’ and the inlet/outlet of the finite domain, this gives

$$-\hat{p} + \frac{\partial \hat{u}}{\partial \hat{r}} = 0 \quad (3.25a)$$

$$\frac{\partial \hat{v}}{\partial \hat{r}} = 0 \quad (3.25b)$$

For the bulk of finite-domain results PTF condition imposed together with a Dirichlet constraint at the inlet. In any given experimental configuration it is unlikely that much control would be available regarding the exact nature of the profile at the inlet to the diverging channel.

The following inlet condition is introduced for diverging channel:

$$\hat{u} = \frac{3}{4\alpha\hat{r}}(1 - \phi^2), \quad \hat{v} = 0 \quad \text{on } \hat{r} = \eta^{-1}, 1 \quad (3.26)$$

The inlet condition in (3.26) is a parabolic flow pattern which is called ‘Diverging Channel Flow’ in present study.

Another inlet and outlet condition is introduced for this channel:

$$\hat{u} = \frac{G'(\phi)}{\alpha\hat{r}}, \quad v = 0 \quad \text{on } \hat{r} = \eta^{-1}, 1 \quad (3.27)$$

The inlet condition in (3.27) is the symmetric Jeffery-Hamel solution.

3.4.2 Hermite-Padé Approximant Solution

The problem defined by equation (3.22) with equation (3.23) is non-linear, for small Channel angle width, one can obtain a series of the form

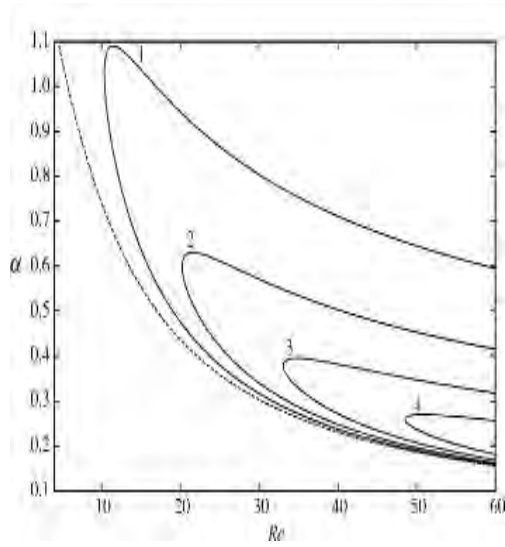
$$G(\phi) = \sum_{i=0}^{\infty} G_i \alpha^i \quad (3.28)$$

Substituting the above expression (3.28) into (3.23) and collecting the coefficients of like powers of α and with the help of MAPLE programming language algebraic system software, first 18 terms for stream-function G is computed in terms of α, Re .

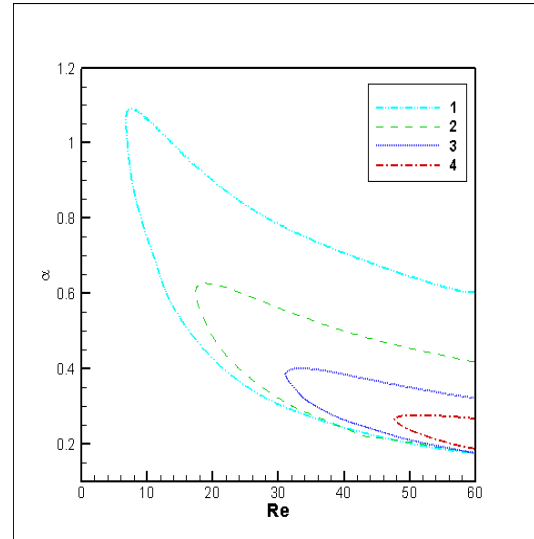
$$G(\phi; \alpha, Re) = \frac{3}{4}\phi - \frac{1}{4}\phi^3 + \left(\frac{3}{4} + \frac{3}{224}Re\right)\phi + \left(-\frac{1}{4} - \frac{33}{1120}Re\right)\phi^3 + \frac{3}{160}Re\phi^5 - \frac{3}{1120}Re\phi^7 \alpha + O(\alpha^3) + \dots \quad (3.29)$$

3.4.3 Validation of numerical scheme

To validate the numerical procedure, the result obtained by the present code is compared with the result of Haines *et al.* [17] for the same problem. The present numerical scheme is validated for the first symmetry-breaking loci of pitchfork bifurcation in the $\alpha - Re$ plane at radius ratio $\eta = 100$ reported by Haines *et al.* [17]. The present result has an excellent agreement with the result obtained by Haines *et al.* [17] which shown in Figure 3.2 are similar.



Haines *et al.* [17]



Present study

Figure 3.2: Code validation of the present research

Based on the above study it is concluded that the numerical scheme applied to the considered problem is reliable. In the next Chapter i.e. in Chapter 4 the result of different parameter's effect on Jeffery-Hamel Flow and Diverging Channel Flow will be analyzed and their bifurcation structure will be discussed.

CHAPTER 4

RESULTS AND DISCUSSION

Stability analysis of Jeffery-Hamel similarity solution and its relation to flow in a diverging channel is analyzed by the controlling parameters channel angle α , Reynolds number Re and radius ratio η . The values of parameters vary as $0 \leq \alpha \leq 1, 0 \leq Re \leq 120, 0 < \eta \leq 100$. The results are represented in terms of velocity profiles, streamlines, and critical relationship for different values of the above parameter in different inlet flow conditions. In the critical relationship $\alpha - Re$ plane, the critical point of Reynolds number \widehat{Re}_c at a fixed angle α and at fixed radius ratio η used to measure the stability of pitchfork bifurcation.

4.1 Effect of angle (α)

The velocity profile of Jeffery-Hamel flow and Diverging Channel flow at different angle α are shown in Figure 4.1, where the radius ratio $\eta = 100$ and Reynolds number $Re = 80$. Figure 4.1 (a) and Figure 4.1 (b) show Diverging Channel flow and Jeffery-Hamel flow respectively at $\alpha = 0.1$ over the finite domain. In the velocity profile at $\alpha = 0.1$, the maximum velocity for Diverging Channel flow is 13.08 and the maximum velocity for Jeffery-Hamel flow is 9.597. Figure 4.1 (c) shows the effect of the velocity profile at $\alpha = 0.17$ for Diverging Channel flow, and the effect of a velocity profile for Jeffery-Hamel flow at $\alpha = 0.17$ are shown in Figure 4.1 (d). At $\alpha = 0.17$, the maximum velocity for Diverging Channel flow is 7.5522 and maximum velocity for Jeffery-Hamel flow is $\alpha = 5.497$. Figure 4.1 (e) shows the velocity profile for Diverging Channel flow at $\alpha = 0.4$ and Figure 4.1 (f) shows the velocity profile for Jeffery-Hamel flow at $\alpha = 0.4$. At $\alpha = 0.4$, the maximum velocity for Diverging Channel flow is 3.454 and the maximum velocity for Jeffery-Hamel flow is 2.398.

Figure 4.1 (g) shows the velocity profile for Divergent Channel flow at $\alpha = 0.7$ and velocity profile for Jeffery-Hamel flow at $\alpha = 0.7$ are shown in Figure 4.1 (h). At $\alpha = 0.7$, the maximum velocity for Diverging Channel flow is 2.307 and the maximum velocity for Jeffery-Hamel flow is 1.370.

It is observed from Figure 4.1, Diverging Channel flow velocity profile is greater than the Jeffery-Hamel flow velocity profile at constant radial volume flux and at fixed radius ratio η . When angle α is increasing, the velocity profile is decreasing for both Diverging Channel flow and Jeffery-Hamel flow.

Figure 4.2 shows the streamlines of Divergent Channel flow and Jeffery-Hamel flow at different angles α with a constant radius ratio η . At angle $\alpha = 0.1, 0.4$ and 0.7 there are no visible differences between streamlines of Divergence Channel flow and streamlines of Jeffery-Hamel flow. At angle $\alpha = 1.39$, the streamlines of Diverging Channel flow are slightly changed with streamlines of Jeffery-Hamel flow. Therefore, it is observed from Figure 4.2, the difference of streamlines change less significantly for smaller channel angles.

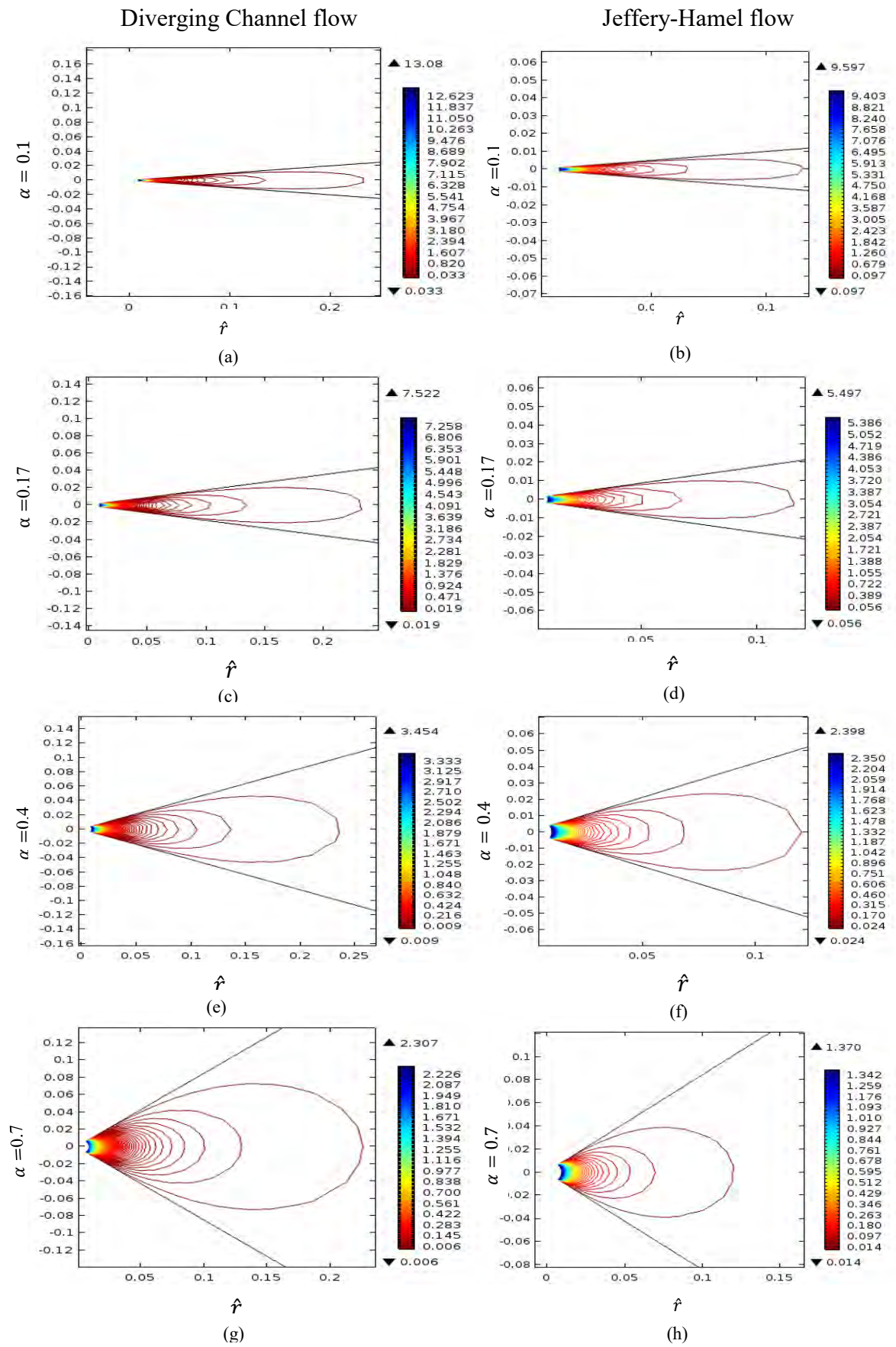


Figure 4.1: Effect of α on velocity profile at $\eta = 100$

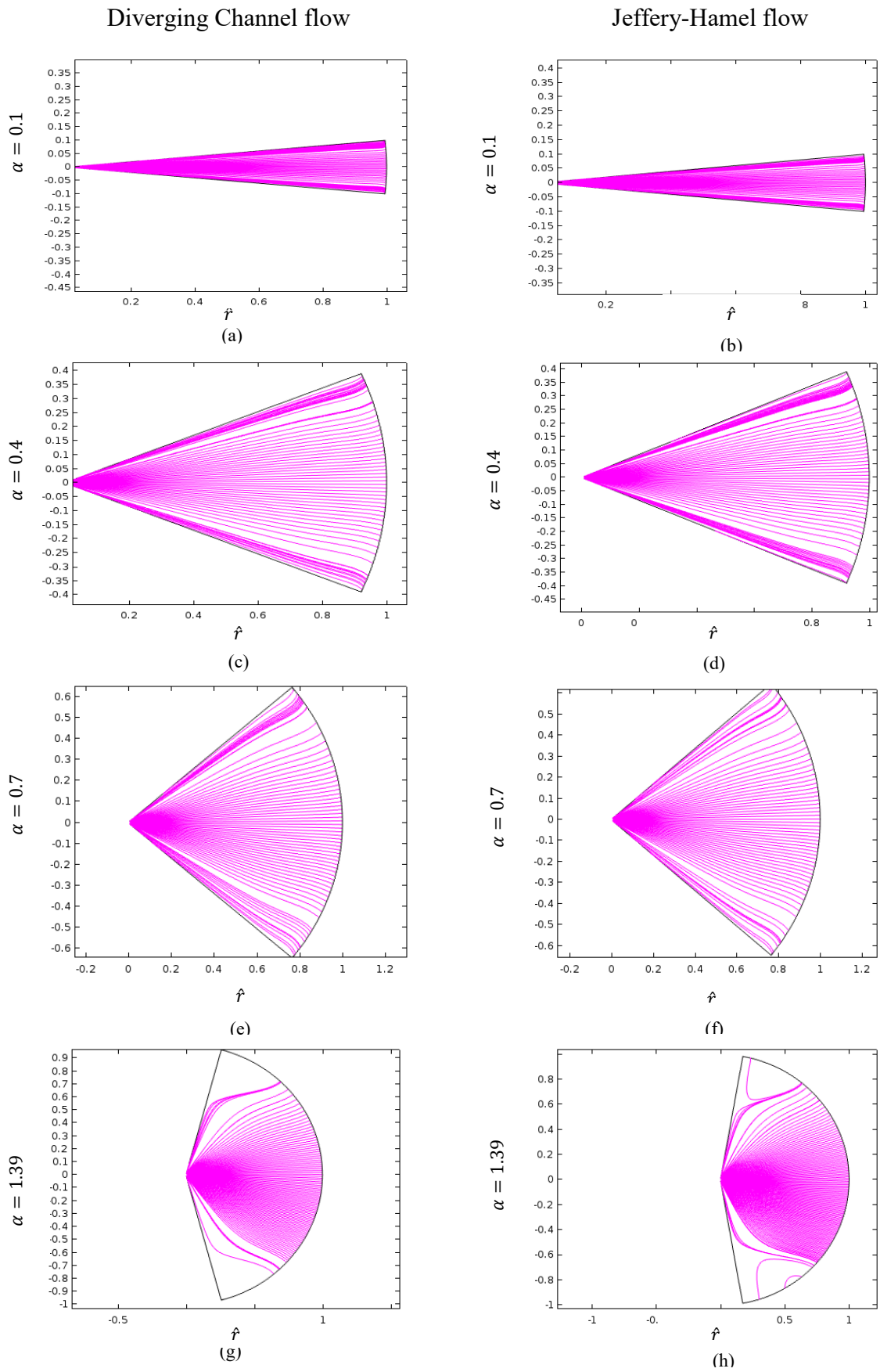


Figure 4.2: Effect of α on streamlines at $\eta = 100$

4.2 Effect of Reynolds number (Re)

Figure 4.3 shows the velocity profile of Jeffery-Hamel flow and Diverging Channel flow at different Reynolds numbers, where fixed angle $\alpha = 0.4$ and radius ratio $\eta = 100$. Figure 4.3 (a) shows the effect of the velocity profile at $Re = 40$ for Diverging Channel flow and effect of velocity profile for Jeffery-Hamel flow at $Re = 40$ are shown in Figure 4.3 (b). At $Re = 40$, maximum velocity for Diverging Channel flow is 3.456 and the maximum velocity for Jeffery-Hamel flow is 2.398. Figure 4.3 (c) shows the velocity profile for Diverging Channel flow at $Re = 80$ and Figure 4.3 (d) shows the velocity profile for Jeffery-Hamel flow at $Re = 80$. The maximum velocity for Diverging Channel flow at $Re = 80$ is 3.457 and the maximum velocity for Jeffery-Hamel flow at $Re = 80$ is 2.410.

Figure 4.3 (e) shows velocity profile for Divergent Channel flow at $Re = 100$ and velocity profile for Jeffery-Hamel flow at $Re = 100$ are shown in Figure 4.3 (f). At $Re = 100$, the maximum velocity for Diverging Channel flow is 3.459 and the maximum velocity for Jeffery-Hamel flow is 2.414. Figure 4.3 (g) shows the velocity profile for Divergent Channel flow at $Re = 120$ and velocity profile for Jeffery-Hamel flow at $Re = 120$ are shown in Figure 4.3 (h). At $Re = 120$, the maximum velocity for Diverging Channel flow is 3.463 and the maximum velocity for Jeffery-Hamel flow is 2.416.

It is observed from Figure 4.3, the velocity profile of Diverging Channel flow is greater than the Jeffery-Hamel flow velocity profile at constant radial volume flux, fixed angle $\alpha = 0.4$ and fixed radius ratio η . When the angle Re is increasing, the velocity profile is also increasing for both Diverging Channel flow and Jeffery-Hamel flow.

Figure 4.4 shows the streamlines of Divergent Channel flow and Jeffery-Hamel flow at different Reynolds number Re with a constant radius ratio $\eta = 100$. At Reynolds number

$Re = 40$ and 80 there are no visible differences between streamlines of Divergence Channel flow and streamlines of Jeffery-Hamel flow. At Reynolds number $Re = 100$ and 120 , the streamlines of Diverging Channel flow are slightly changed with streamlines of Jeffery-Hamel flow. Therefore, it is observed from Figure 4.4, the difference of streamlines change less significantly for low Reynolds numbers.

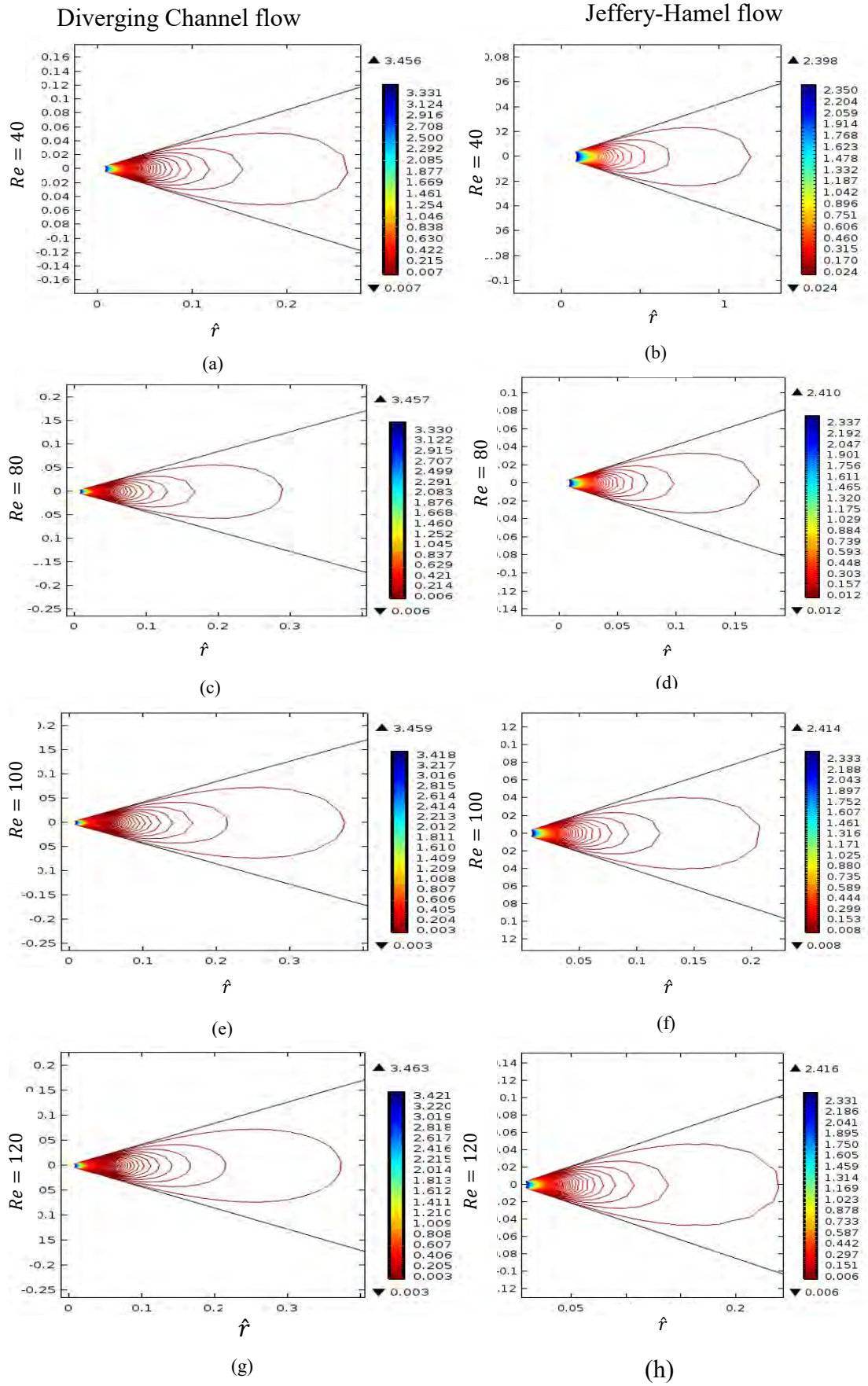


Figure 4.3: Effect of Re on velocity profiles

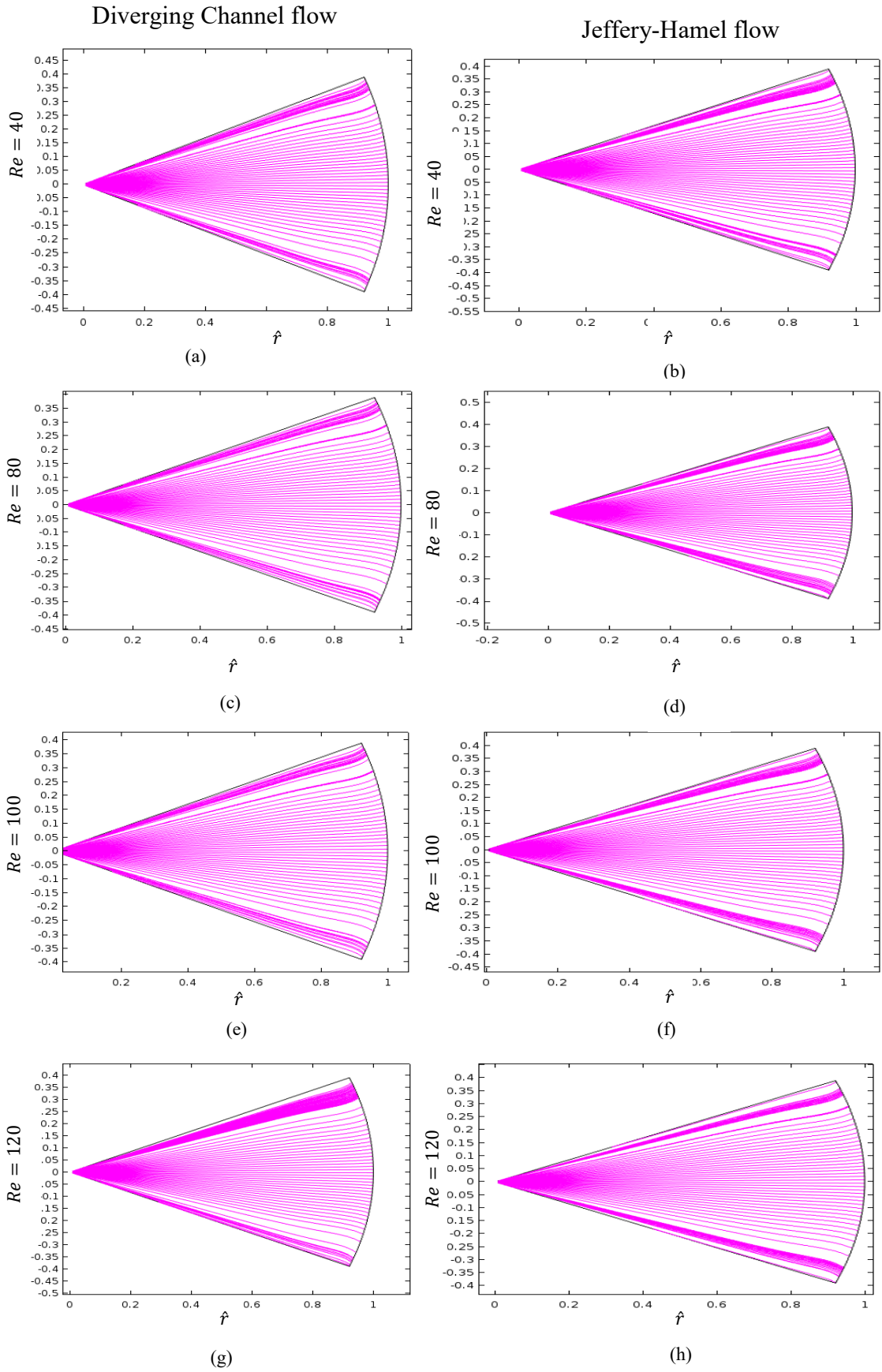


Figure 4.4: Effect on Re on streamlines

4.3 Effect of radius ratio (η)

Radius ratio η has a significant effect on velocity profile of Diverging Channel flow and velocity profile of Jeffery-Hamel flow over the physical domain. Figure 4.5 shows the velocity profile of Jeffery-Hamel flow and Diverging Channel flow at different radius ratio η , where fixed angle $\alpha = 0.4$ and constant Reynolds number Re . Figure 4.5 (a) shows the effect of velocity profile at $\eta = 100$ for Diverging Channel flow and effect of velocity profile for Jeffery-Hamel flow at $\eta = 100$ are shown in Figure 4.5 (b). At $\eta = 100$, maximum velocity for Diverging Channel flow is 3.307 and maximum velocity for Jeffery-Hamel flow is 2.414. Figure 4.5 (c) shows velocity profile for Diverging Channel flow at $\eta = 50$ and Figure 4.5 (d) shows velocity profile for Jeffery-Hamel flow at $\eta = 50$. Maximum velocity for Diverging Channel flow at $\eta = 50$ is 1.653 and maximum velocity for Jeffery-Hamel flow at $\eta = 50$ is 1.208. Figure 4.5 (e) shows velocity profile for Divergent Channel flow at $\eta = 20$ and velocity profile for Jeffery-Hamel flow at $\eta = 20$ are shown in Figure 4.5 (f). At $\eta = 20$, the maximum velocity for Diverging Channel flow is 0.661 and the maximum velocity for Jeffery-Hamel flow is 0.483. Figure 4.5 (g) shows velocity profile for Divergent Channel flow at $\eta = 10$ and velocity profile for Jeffery-Hamel flow at $\eta = 10$ are shown in Figure 4.5 (h). At $\eta = 10$, the maximum velocity for Diverging Channel flow is 0.333 and the maximum velocity for Jeffery-Hamel flow is 0.241. It is observed from Figure 4.5, velocity profile of Diverging Channel flow is greater than Jeffery-Hamel flow velocity profile at constant radial volume flux, fixed angle $\alpha = 0.4$ and constant Reynolds number $Re = 100$. When radius ratio η is decreasing, the velocity profile is also decreasing for both Diverging Channel flow and Jeffery-Hamel flow. Figure 4.6 shows the streamlines of Divergent Channel flow and Jeffery-Hamel flow at different radius ratio η . At $\eta = 100, 50, 20, 10$; the streamlines of Diverging Channel flow are slightly changed with streamlines of Jeffery-Hamel flow.

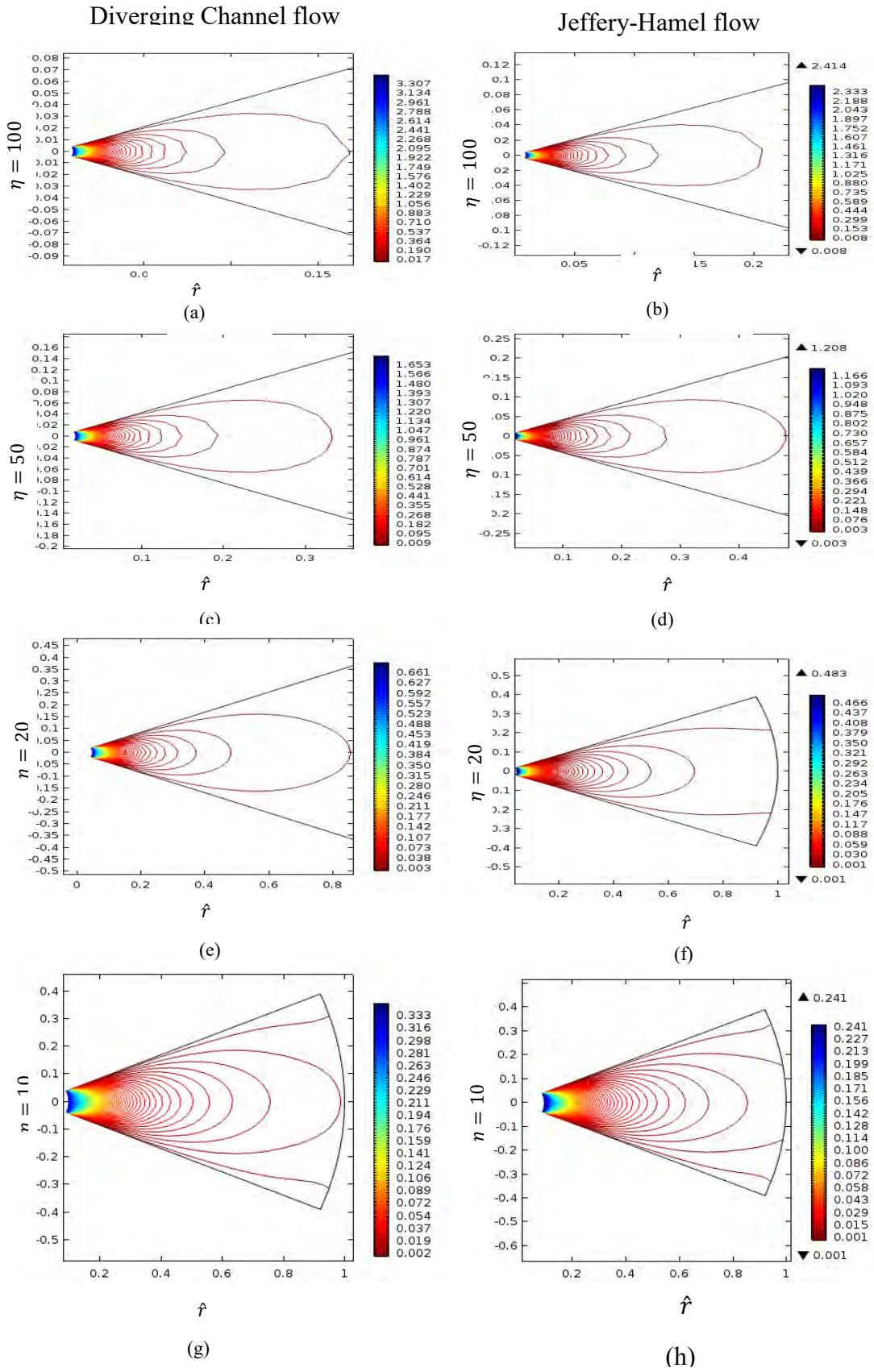


Figure 4.5: Effect of η on velocity profiles

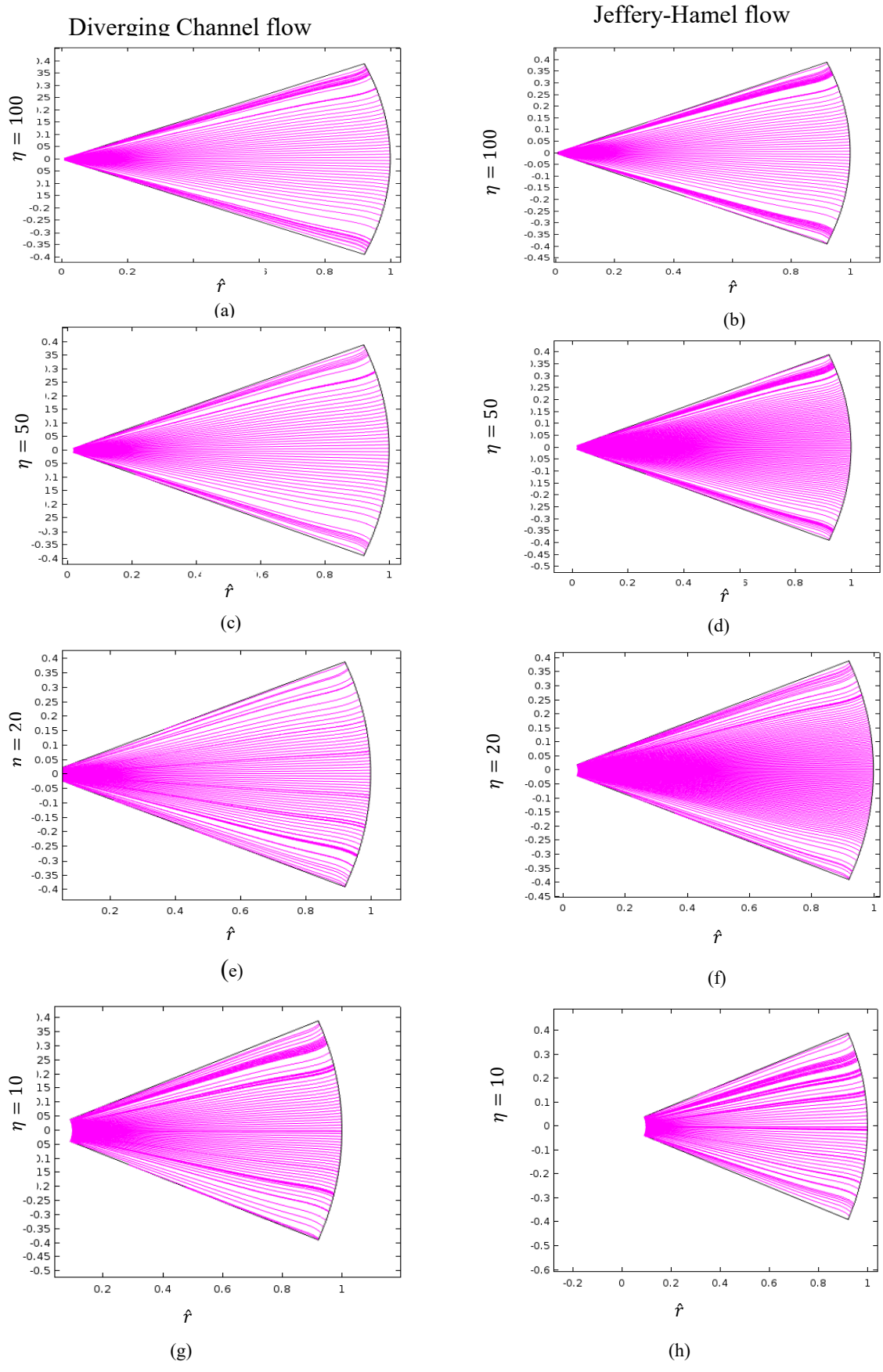


Figure 4.6: Effect of η on streamlines

4.4 The Bifurcation Structure in Finite Domain

In this section, all results are presented for the inlet boundary condition and outlet boundary condition of the physical domain. For these conditions, the computational task is to locate pitchfork bifurcation with a critical points in the $\alpha - Re$ plane at a fixed radius ratio η . Once a critical point has been located, its locus in the $\alpha - Re$ plane can be determined. These critical points are obtained by forming the appropriate system, which ensures that the solution lies exactly at the bifurcation point. Figure 4.7 shows the pitchfork bifurcations found for $\eta = 100$ and $0 \leq Re \leq 60$. An infinite number of critical relationship diagrams can be found in the combined limit of $\alpha \ll 1$, $Re \gg 1$ and $\eta \gg 1$. Figure 4.7 shows that the pitchfork bifurcation is ‘right facing’ in the sense that the resulting symmetry-broken flows exist for $Re > \widehat{Re}_c(\alpha)$ in all cases. Here a hat notation is introduced, \widehat{Re}_c , to distinguish critical Reynolds numbers of the finite domain from that associated with the Jeffery-Hamel pitchfork bifurcation. Figure 4.7 (a) shows the critical Reynolds number of the bifurcation diagram is $\widehat{Re}_c \approx 7.503265$ at a separation angle $\alpha = 1.0472$. Figure 4.7 (b) shows at a separation angle $\alpha = 0.619465$, the critical Reynolds number is $\widehat{Re}_c \approx 17.70995$. At a separation angle $\alpha = 0.379416$, critical Reynolds number $\widehat{Re}_c \approx 31.1227$ is found in Figure 4.7 (c). Critical Reynolds number $\widehat{Re}_c \approx 47.6353$ is found at separation angle $\alpha = 0.26278$ in Figure 4.7 (d). It is observed from Figure 4.7 that the pitchfork bifurcations in a finite domain are in good quantitative agreement with the boundary \mathcal{B}_2 predicted by the infinite domain similarity solution.

Figure 4.8 shows the critical relationship of $\alpha - Re$ plane for $0 \leq Re \leq 120$. These relationships can be obtained by employing Hermite-Padé Approximation method. The critical relationship shows in Figure 4.8 (a) indicates the variation of the Reynolds number at which the critical point of isolated solutions exists for varying channel angles α . Figure

4.8 (b) shows the solution \mathcal{B}_1 at a fixed angle $\alpha = 0.28$ which indicates that the existence of the isolated solution \mathcal{B}_1 is $Re \approx 40$ at $\eta = 100$.

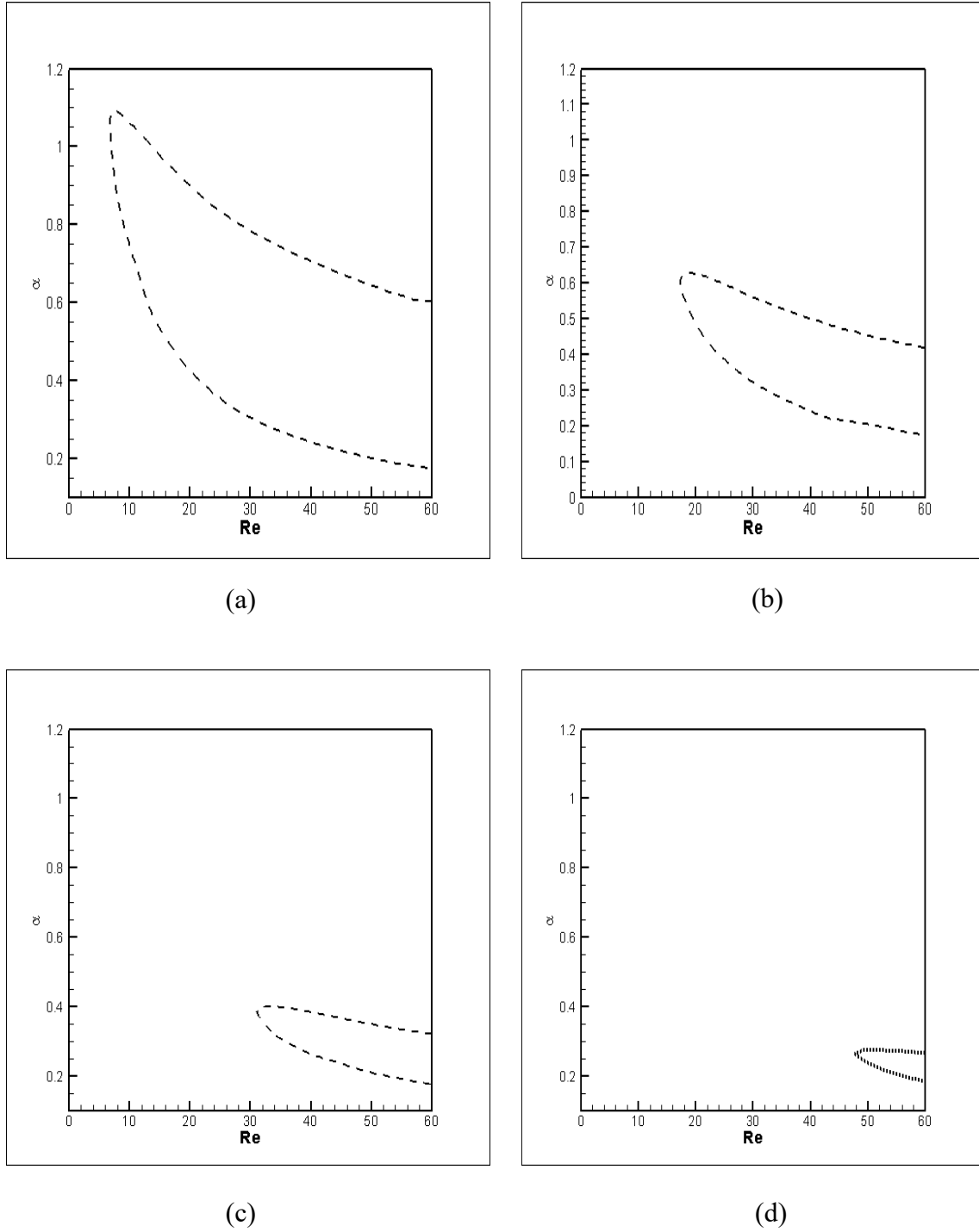


Figure 4.7: Critical relationship in the $\alpha - Re$ plane for $0 \leq Re \leq 60$

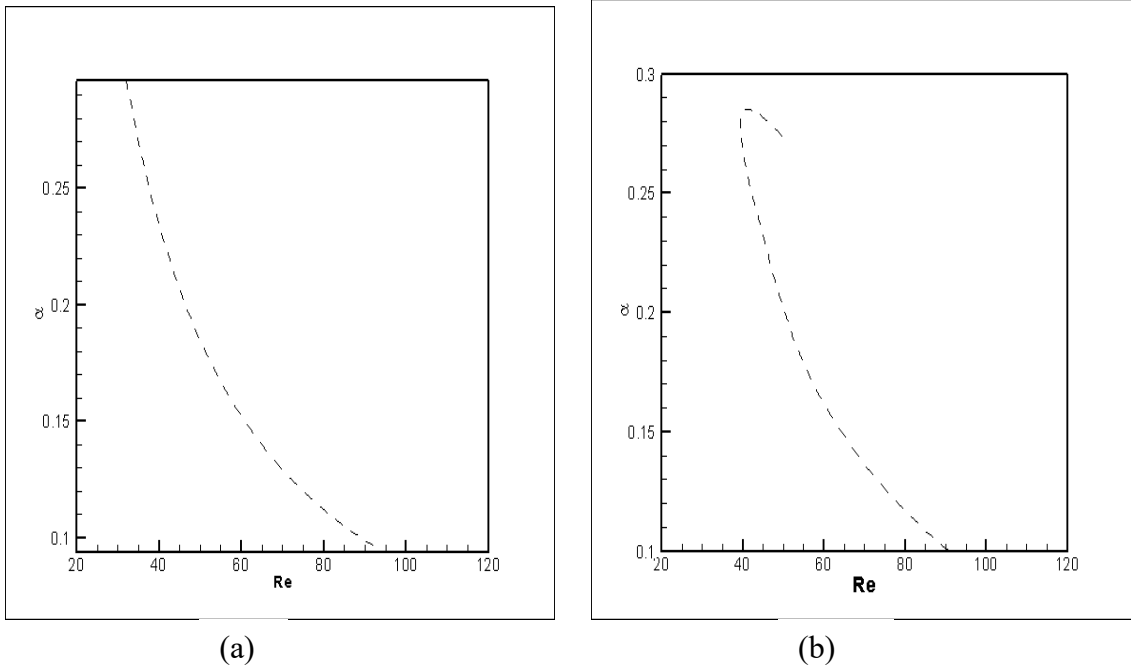


Figure 4.8: Critical relationship in $\alpha - Re$ plane for $20 \leq Re \leq 120$

4.5 The Physical Relevance of Numerical results

In the previous sections, a comprehensive picture of solution structure has been presented for a specific choice of boundary conditions. The practical relevance of these results requires that: (i) the solutions are stable; (ii) the domain is experimentally realizable; (iii) there is no strong sensitivity to inlet/outlet constraints.

Table 4.1: The variation of the critical Reynolds \widehat{Re}_c number of the symmetry-breaking bifurcation in a finite domain

α	Jeffery-Hamel flow \widehat{Re}_c	Diverging Channel flow \widehat{Re}_c	Hanies et al. [17] \widehat{Re}_c	
			Jeffery-Hamel flow	Diverging Channel flow
0.1	94.179954	94.71643	94.18	94.72
0.4	23.270214	23.76458	23.27	23.77
0.7	12.8502	13.7032	12.85	13.72

Table 4.1 shows, two different inlet profiles at a different angle α for $\eta = 100$ and their influence on the finite-domain base flow which is rather minimal. The variation in the inlet profile leads to a variety of critical Reynolds number \widehat{Re}_c which is less than 1% at $\alpha = 0.1$ when $\eta = 100$. The influence of the inlet profile is stronger for wider expansion angles. The change in critical Reynolds number is approximately 8% at $\alpha = 0.7$ when $\eta = 100$. So the solution structure is less sensitive to outflow conditions.

In the next Chapter, the result analysis of the present study is summarized.

CHAPTER 5

CONCLUSION

The effect of angle (α), Reynolds number (Re), and radius ratio (η) on the flow structure of Jeffery-Hamel flow and Divergent Channel flow has been analyzed numerically. The various ideas and results have been discussed in detail at the relevant Chapter of the thesis. A related geometry is investigated which has long parallel inlet/outlet channels and recovered the qualitative behavior that is described. The governing equations are solved by the Finite Element Method (FEM) and also solved by the Hermite-Padé Approximant method to find $\alpha - Re$ relation which is also good agreement with published data. The present investigation of the finite domain computational problem concluded that the choice of inlet/outlet conditions has a limited impact on the similarity solution behavior. Furthermore, there is a good agreement between Jeffery-Hamel Flow and Diverging Channel Flow over the domain.

5.1 Summary of the Major Outcome

From the investigation the following conclusion has been drawn:

- ❖ At a separation angle of $\alpha = 0.1$ the pitchfork bifurcation occurs at $\widehat{Re}_c \approx 94.71643$. Also at a separation angle $\alpha = 0.4, 0.7$ the pitchfork bifurcation occurs at $\widehat{Re}_c \approx 23.270214, 12.8502$. For $Re > \widehat{Re}_c$ the solution is found to be unstable.
- ❖ The parameter α, Re, η has a significant impact on the velocity distribution of both Jeffery-Hamel flow and Divergence Channel flow. When angle α is increasing, the fluid velocity in the radial direction is decreasing, with the increasing of Reynolds number Re the fluid velocity in the radial direction is

increasing and with the decreasing of η , fluid velocity in the radial direction is decreasing.

- ❖ The difference induced by changes in inlet conditions becomes less significant for smaller channel angles.
- ❖ In the finite domain the Jeffery-Hamel flow has a sequence of pitchfork bifurcations in the limit of $Re \gg 1$ and $\alpha \ll 1$.

FUTURE WORK

The following can be put forward to the further works as follows-ups of the present research as

- ❖ The study can be extended by including different physics like internal heat generation/absorption.
- ❖ Investigation can be analyzed by using magnetic fluid.
- ❖ Study can be continued by changing the boundary conditions of the inlet/outlet walls.
- ❖ The study can be extended for unsteady flow with periodic conditions.
- ❖ The study can be extended for Nano-fluids.
- ❖ Only two-dimensional fluid flow is performed in this thesis. So this deliberation may be extended to three-dimensional dimensional analysis to investigate the effects of different parameters.

References

- [1] Jeffery, G. B., (1915), Two-dimensional Steady Motion of a Viscous Fluid, *Philosophical Magazine*, vol. 6, pp. 455-465.
- [2] Hamel, G., (1916), Spiralförmige Bewegungen Zäher Flüssigkeiten, *Jahresbericht der Deutschen Math. Vereinigung*, vol. 25, pp. 34-60.
- [3] Batchelor, G. K., (1967), *An Introduction to Fluid Dynamics*, Cambridge University Press, Cambridge.
- [4] Schlichting, H., (2000), *Boundary-layer Theory*, McGraw-Hill Press, New York.
- [5] Drazin, P. G., (1992), *Nonlinear System*, Cambridge University Press.
- [6] Alam, M. S., (2009), *Critical Behaviour of Hydromagnetic Flows in Convergent-Divergent Channels*, M.Phil. Thesis, BUET.
- [7] Rosenhead, L., (1940), The Steady Two-dimensional Radial Flow of Viscous Fluid between Two Inclined Plane Walls, *Proceedings of the Royal Society of London*, vol. A175, pp. 436-467.
- [8] Fraenkel, L. E., (1962), Laminar Flow in Symmetrical Channels with Slightly Curved Walls, I: On the Jeffery-Hamel Solutions for Flow between Plane Walls, *Proceeding of the Royal Society of London*, vol. A267, pp. 119-138.
- [9] Banks, W. H. H, Drazin, P. G., and Zaturka, M. B., (1988), On Perturbations of Jeffery-Hamel Flow, *Journal of Fluid Mechanics*, vol. 186, pp. 559-581.
- [10] Dean, W. R., (1934), Note on the Divergent Flow of Fluid, *Philosophical Magazine*, vol. 18(7), pp. 759-777.
- [11] Goldshitik, M., Hussain, F., and Shtern, V., (1991), Symmetry Breaking in Vortex-sources and Jeffery-Hamel Flows, *Journal of Fluid Mechanics*, vol. 232, pp. 521-566.

- [12] Dennis, S. C. R, Banks, W. H. H., Drazin, P. Z., and Zaturaska, M. B., (1997), Flow along a Diverging Channel, *Journal of Fluid Mechanics*, vol. 336, pp. 183-202.
- [13] Sobey, I. G., and Drazin, P.G., (1986), Bifurcation of Two-dimensional Channels Flows, *Journal of Fluid Mechanics*, vol. 171, pp. 263-287.
- [14] Hemadiche, M., Scott, J., and Jeandel, D., (1994), Temporal Stability of Jeffery-Hamel Flow, *Journal of Fluid Mechanics*, vol. 268, pp. 71-88.
- [15] Putkaradze, V., and Vorobieff, P., (2006), Instabilities, Bifurcations and Multiple Solutions in Expanding Channel Flows, *Physical Review Letters*, vol. 97 (14), pp. 144502.
- [16] Tutty, O. R., (1996), Nonlinear Development of Flow in Channels with Non-parallel Walls, *Journal of Fluid Mechanics*, vol. 326, pp. 265-284.
- [17] Haines, P. E., Hewitt R. E., and Hazel, A. L., (2011), The Jeffery Hamel Similarity Solution and Its Relation to Flow in a Diverging Channel, *Journal of Fluid Mechanics*, vol. 687, pp. 404-430.
- [18] Kuznetsov, Y. A., (2004), *Elements of Applied Bifurcation Theory*, New-York: Springer-Verlag.
- [19] Strogatz S. H., (1996), *Nonlinear Dynamics and Chaos*, Addison Wesley Publication Company.
- [20] Wiggins, S., (1990), *Introduction to Applied Nonlinear Dynamical Systems and Chaos*, New-York: Springer.
- [21] Cengul, Y. A., and Cimbala, J. M., (2014), *Fluid Mechanics: Fundamentals and Applications*, McGraw-Hill.
- [22] Chung, T. J., (2002), *Computational Fluid Dynamics*, Cambridge University Press, Cambridge.

- [23] Ferziger, J. H., and Perić, M., (1997), Computational Methods for Fluid Dynamics, Springer Verlag, Berlin Heidelberg.
- [24] Dechaumphai, P., (1999), Finite Element Method in Engineering, Chulalongkorn University Press, Bangkok.
- [25] Reddy, J. N., and Gartling, D. K., (1994), The Finite Element Method in Heat Transfer and Fluid Dynamics, CRC Press, Boca Raton, Florida.
- [26] Sayma, A., (2009), Computational Fluid Dynamics, Ventus Publishing ApS.
- [27] Baker, G. A. Jr. and Graves-Morris, P., (1996), Padé Approximant, Cambridge University Press, Cambridge.
- [28] Mankinde, O. D., (2005), Approximation Approach to Hydro-magnetic Flows in Convergent-Divergent Channels, The Abdus Salam International Centre for Theoretical Physics, Trieste, Italy.
- [29] Khan, M. A. H., (2002), Higher-Order Differential Approximants, Journal of Computational and Applied Mathematics, vol. 149, pp. 457-468.